Icarus 329 (2019) 101–123

Contents lists available at ScienceDirect

Icarus

journal homepage: www.elsevier.com/locate/icarus

Mapping Europa's microfeatures in regional mosaics: New constraints on formation models

J.L. Noviello[a,*], Z.A. Torrano[a], A.R. Rhoden[a,b], K.N. Singer[b]

[a] School of Earth and Space Exploration, Arizona State University, Tempe, AZ 85287, United States of America
[b] Southwest Research Institute, Boulder, CO, United States of America

A B S T R A C T

Europa is an unusual world, and its surface features provide clues as to how it has evolved. We mapped, characterized, and analyzed small ($\leq 100\,km^2$ in area) endogenic features on Europa's surface in order to identify patterns among and within different types of features and provide observational tests for formation models. To create a fully digitized and validated data set of these microfeatures, we merged data sets obtained by previous mapping studies that focused on small chaos, domes, pits, spots, and hybrid features in moderate resolution (~230 m/pix) images of Europa, including the four main regional map areas. We expanded upon the definition of a recently-identified feature definition type, here called hybrids, and suggest more quantitative metrics for describing pits, spots, domes, and microchaos. Across all four regions mapped, we find that microchaos are the most numerous, followed by pits and domes, respectively. Spots are the least common features, and the smallest, which might indicate an observational bias, as they may contain disruptions smaller than what is visible at this scale. Microchaos features are, on average, larger and darker than all other microfeature types. We compare our observations to the findings and predictions of previous numerical modeling studies, and suggest that the observations are most consistent with cryovolcanism and liquid water sill models. While no one model is able to explain all the observations, there are elements of each that should be considered in future modeling studies.

1. Introduction

Europa's surface is peppered with hundreds of endogenic features including chaos features, which are present across a large range of sizes, and small features collectively referred to as lenticulae. Chaos features are defined as irregular polygons with a hummocky or platy interior texture and are often but not always associated with areas of low albedo (Greenberg et al., 1999; Prockter et al., 1999; Greeley et al., 2000; Figueredo et al., 2002) and a higher concentration of salts (Hand and Carlson, 2015). The rafts inside of platy chaos features are the remains of previous terrain that the chaos feature disrupted during its formation. Chaos features have been extensively studied in terms of their morphology (Head et al., 1999; Greenberg et al., 1999; Spaun, 2002; Figueredo et al., 2002; Collins and Nimmo, 2009; Singer et al., in review), potential formation mechanisms (Head and Pappalardo, 1999; Greeley et al., 2000; Riley et al., 2000; Spaun, 2002; Figueredo et al., 2002; Collins and Nimmo, 2009; Schmidt et al., 2011), locations and clustering (Greenberg et al., 1999; Spaun et al., 1999; Riley et al., 2000; Soderlund et al., 2014; Culha and Manga, 2016; Leonard et al., 2017; Noviello et al., 2017), observational constraints (Neish et al., 2012; Bunte, 2013; Noviello and Rhoden, 2018; Leonard et al., 2018), and relation to Europa's geologic history (Pappalardo et al., 1999; Head and Pappalardo, 1999; Prockter et al., 1999; Greeley et al., 2000; Spaun, 2002; Greenberg et al., 2003; Figueredo and Greeley, 2004; Spaun et al., 2004; Collins and Nimmo, 2009; Schmidt et al., 2011; Leonard et al., 2018; Singer et al., in review). This terrain type is estimated to cover between 20% (Figueredo and Greeley, 2004) and 40% (Riley et al., 2000) of Europa's surface. Chaos is easily identifiable in the moderate resolution (220–230 m/pix) images of Europa across most lighting angles (Neish et al., 2012), enabling detailed data collection efforts across ~10% of Europa's surface (Doggett et al., 2009; Neish et al., 2012). Large chaos features are visible in low resolution (≥ 1.5 km/pix) images (Neish et al., 2012), so these features have been mapped globally (Riley et al., 2000; Bunte, 2013; Leonard et al., 2017), but little is known about their details or the global distribution of any other non-linear feature type.

Other features occur alongside chaos, and have been subdivided into specific types (Pappalardo et al., 1998; Greeley et al., 2000; Figueredo and Greeley, 2004; Spaun, 2002; Greenberg et al., 2003; Collins and Nimmo, 2009; Culha and Manga, 2016) primarily based on qualitative assessment of their morphologies (Fig. 1). Small chaos (microchaos) are small areas with disrupted terrain and often irregular edges (Fig. 1A). Uplifts and domes are features with positive relief (Fig. 1B; Greeley et al., 2000; Greenberg et al., 2003; Singer et al., 2010). Uplifts are usually more polygonal, while domes are more elliptical. Pits are generally elliptical features with negative

* Corresponding author at: School of Earth and Space Exploration, Arizona State University, ISTB4 Room 765, 781 E. Terrace Mall, Tempe, AZ 85287, United States of America.
E-mail address: JLNoviel@asu.edu (J.L. Noviello).

https://doi.org/10.1016/j.icarus.2019.02.038
Received 11 October 2018; Received in revised form 22 February 2019; Accepted 27 February 2019
Available online 21 March 2019
0019-1035/

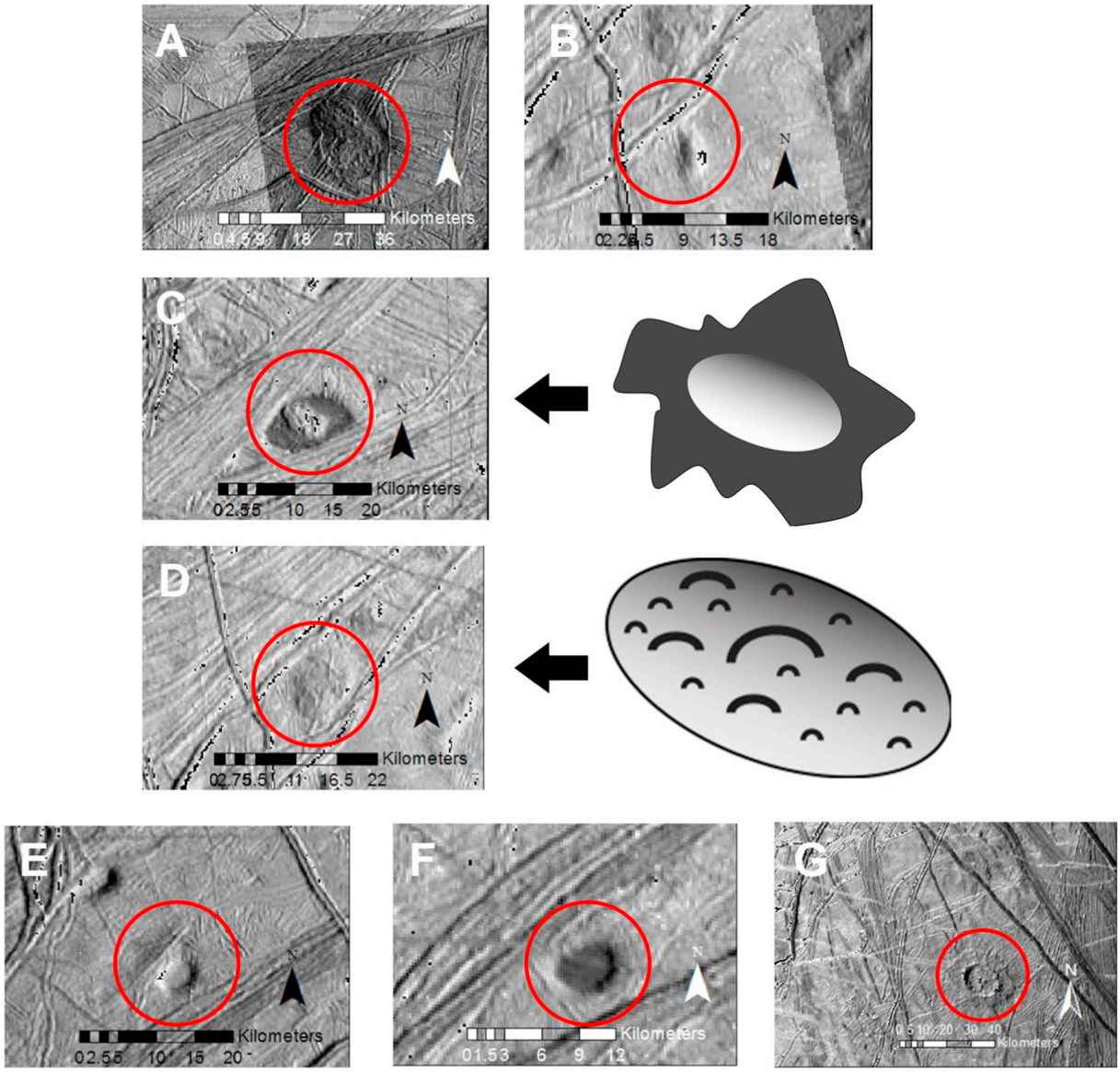

Fig. 1. Microfeatures.
Examples of microfeatures seen in the four RegMaps on Europa's surface. A) Chaos, classified as such by the hummocky interior and clear disruption of the previous terrain (sun from right). B) A dome, characterized by its positive topography (sun from right). C) Type I hybrid morphology, characterized by a positive topographic feature inside of a dark "halo" (sun from right). The halo can be smooth or have a hummocky appearance. D) Type II hybrid morphology, characterized by a positive topographic feature with a fully disrupted surface, akin to the hummocky interior of the chaos feature in A (sun from bottom right). The visible cracks are inconsistent with the surrounding terrain. E) A pit, characterized by its negative topography (sun from top left). F) A spot, characterized by consistent albedo and lack of interior disruption (sun from bottom right). G) A crater on Europa (sun from top left).

topographical relief (Fig. 1E; Greeley et al., 2000; Greenberg et al., 2003; Singer et al., 2010; Singer et al., in review). Spots are elliptical areas that have low albedo, but without any discernable interior structure (i.e. a hummocky interior or rafts) and no obvious topography (Fig. 1F; Greeley et al., 2000; Greenberg et al., 2003; Singer et al., 2010; Singer et al., in review). A recent mapping study of selected regions of Europa revealed an additional category of hybrid features, in which a distinct dome or uplift is present within a chaos feature (Fig. 1C and D; Culha and Manga, 2016). Some of these features had previously been considered domes or uplifts with cracked surfaces (Rathbun et al., 1998; Greenberg et al., 2003; Quick et al., 2017), but not until recently were they considered a separate type. Much of the literature refers to these features, especially pits, spots, and domes, as lenticulae. This language is avoided here, so as not to exclude small chaos features and to emphasize that not all of these features studied are albedo features.

The process of chaos formation disrupts and transforms the previous terrain. This can be interpreted as evidence that some kind of melting is involved, implying the presence of liquid water or warm ice near Europa's surface. Initial models for chaos formation invoked full melt through of a thin ice shell (Greenberg et al., 1999; Collins et al., 2000; O'Brien et al., 2002; Nimmo and Giese, 2005) or a warm-ice diapir rising through a thick ice shell (Pappalardo et al., 1998; Figueredo et al., 2002; Schenk and Pappalardo, 2004; Showman and Han, 2005; Singer et al., 2010; Soderlund et al., 2014; Singer et al., in review). These two models explained some characteristics of chaos features, but there remained other aspects that neither model could fully explain (Collins and Nimmo, 2009).

A more recent model, specifically designed to address the formation of large chaos features, invokes local melt water formed by a rising diapir that disaggregates the overlying ice (Schmidt et al., 2011). As the convective plume reaches its minimum depth in the ice shell, the overlying surface is deflected downward to compensate for the decrease

in volume caused by the ice melting into a liquid melt lens. As the melt lens begins to collapse, ice blocks cleave off from the surrounding ice shell. As the water lens refreezes, the blocks above rotate, and domes form in between the disrupted ice blocks and at the margins of hummocky chaos. This mandates that the sill is much larger than the domes themselves, as the domes form in between the large ice blocks. It is not clear if this method of dome formation can account for domes that appear isolated, or if it necessitates that domes must be clustered above the location of the sill. The work also briefly notes that the scale of the ascending plumes and the preexisting terrain accounts for the range of chaos morphologies, and could explain domes, but does not explain pits or spots. Finally, while the model can explain the formation of larger chaos features such as Conamara and Thera Macula, it is unclear if this model could be applied to microchaos (chaos under 100 km^2 in area) or any of the microfeatures. As our work is focused on microfeatures, we do not consider the details of the Schmidt model, but we do include it in the suite of models that invoke liquid water in the formation of surface features. Another liquid water model, discussed in more detail later, specifically focuses on microfeatures and their relationship to each other (Manga and Michaut, 2017); we explore this model in more detail.

The similar range of sizes and clustering patterns of small chaos features, domes, pits, and spots have led to the hypothesis that they may be genetically related (Pappalardo et al., 1998; Rathbun et al., 1998; Collins and Nimmo, 2009; Singer et al., 2010; Schmidt et al., 2011; Michaut and Manga, 2014; Manga and Michaut, 2017; Noviello et al., 2017; Singer et al., in review). Understanding how one forms could lead to an understanding of the entire microfeature formation process. Similar to large chaos features, one proposed mechanism for microfeature formation is solid-state convection, in which a warm-ice diapir rises through Europa's ice shell (Pappalardo et al., 1998; Rathbun et al., 1998). The warm ice will rise until it reaches a point of neutral buoyancy, at which point it will begin to spread out laterally. Additional studies have suggested that variations of this process could partially melt the ice above the diapir's head, either due to localized compositional impurities and brine mobilization (Head and Pappalardo, 1999; Pappalardo and Barr, 2004) or from the localized effects of tidal heating (Sotin et al., 2002). Further work demonstrated that tidal heating can enhance the effects of partial melting (Sotin et al., 2002; Mitri and Showman, 2008; Han and Showman, 2010), which may concentrate melt within the diapir, creating chaos and potentially other microfeature types.

Another proposed mechanism for forming microfeatures involves liquid water rather than warm ice (Schmidt et al., 2011; Manga and Michaut, 2017). In this model, an over-pressurized ocean (Manga and Wang, 2007; Michaut and Manga, 2014) pushes liquid into Europa's ice shell via a conduit or a pre-existing fracture (Quick and Marsh, 2016; Craft et al., 2016; Culha and Manga, 2016; Manga and Michaut, 2017). The liquid water eventually reaches a point of neutral buoyancy within the ice shell, and spreads out laterally to form a subsurface volume of liquid water (i.e. a sill). The mass influx from the liquid water and subsequent freezing changes the water volume and, consequently, the morphology at the surface. Different stages of the sill's evolution can cause different microfeatures to form on the surface above it. Early in the process, a pit or dome forms, depending on how the liquid water pocket is compensated (Manga and Michaut, 2017). Then during freezing, either a dome forms (Schmidt et al., 2011; Manga and Michaut, 2017), or the surface is breached to form a chaos feature (Manga and Michaut, 2017), depending on whether or not part of the weight is supported by elastic flexure in the ductile upper ice shell.

More recent work (Quick and Marsh, 2016; Quick et al., 2017) has examined the possibility that some domes are the result of cryovolcanism on Europa. Previous studies (Rathbun et al., 1998; Pappalardo and Barr, 2004) have noted that domes can present in slightly different morphologies; some are texturally different material from the surrounding plains, typically with a lower albedo. These domes may also occur with surrounding "moats" of lower albedo, which may be more consistent with hybrid features. The other type of domes retains the pre-existing terrain on the upwarped surfaces (called "punched through" in Quick et al., 2017). The domes that retain the original terrain may have been created as the result of viscous extrusions of cryolava onto Europa's surface (Quick et al., 2017), an idea expressed earlier for the large chaos feature Murias chaos (Figueredo et al., 2002). Cryovolcanism can also explain the dark "moats" around some of the hybrid features, as it is merely the extent of the cryolava flow. If correct, cryovolcanism can potentially explain both hybrid features and domes, and may even explain bands and ridges as manifestations of subsurface cryomagmatic processes associated with diapirism (Quick and Marsh, 2016).

Each of these proposed formation mechanisms is associated with predictions and assumptions for microfeature characteristics, which we discuss in detail in Section 4.2. Hence, geographical and morphological information about microfeatures can help constrain their formation mechanism. Chaos clustering near the poles could imply that tidal heating is necessary to form chaos (Collins and Nimmo, 2009), while a more random or dispersed global distribution could implicate sills, as they could form anywhere. Although microfeatures have been mapped in several studies, there is significant variation between individual mapping data sets, especially as technology has improved to allow for more quantitative studies to be conducted.

Having one complete, validated geomorphic map of microfeatures on Europa that represents all previous work can facilitate discussions regarding feature distribution, size, and morphologies, and could help form and focus science objectives for the upcoming Europa Clipper mission (Phillips and Pappalardo, 2014; Pappalardo et al., 2016). To fulfill this need, we have produced a geomorphic map of Europa's microfeatures, including small chaos features ($\leq$100 km^2), and merged it with three previous maps (Greenberg et al., 2003; Culha and Manga, 2016; Singer et al., in review) to create a validated, digitized map of microfeatures on Europa within the regional mosaics ("RegMaps") that cover ~10% of the surface. Next, we have obtained morphological information for each feature, including area, diameter, and normalized reflectance. Finally, we have presented our observational findings and their implications for formation models. Our work seeks to improve our understanding of how Europa's microfeatures form, and assess whether different types of features form in related or distinct processes, by identifying statistically significant morphologic indicators of each type. This work presents new constraints that future modeling efforts on microfeature formation should address and serves as the basis for future work on quantitative classification of these features.

2. Materials and methods

2.1. Data and mapping

All the images used in this study came from the *Galileo* SSI instrument. Only images taken with the clear filter (611 nm; Belton et al., 1992) were used. Images were taken in *Galileo*'s 15th and 17th orbits, both of which had Europa as its central target; these images make up the regional map mosaics. Table 1 shows the average image characteristics for the images included in each RegMap; for details of each image used, see Appendix A. This data set enables mapping of both the northern (0° to 55°N) and southern (0° to 65°S) latitudes at two separate longitudes (~90°W and ~230°W) on Europa.

Because the resolutions of regional mapping images were degraded for inclusion in the USGS basemap of Europa (USGS, 2002), we chose to import the raw *Galileo* images and tie them to the basemap at full resolution, which involved a series of steps. First, the raw regional mapping images were downloaded from the Planetary Data System (PDS) and converted into cube files for processing using the open-source United States Geological Survey (USGS) software ISIS3 (Torson and Becker, 1997; Anderson et al., 2004). Pointing information was

Table 1
Details about the average characteristics of the images used to create the RegMaps used in this study. More information regarding individual images are found in Appendix B.

Region	Average resolution (m/px)	Average phase angle (deg)	Average emission angle (deg)	Average incidence angle (deg)
E15RegMap01	231.12	63.15	37.60	77.46
E15RegMap02	237.33	100.54	37.47	78.12
E17RegMap01	218.20	72.35	20.30	77.92
E17RegMap02	222.31	92.62	28.15	79.51

attached to the raw cubes and basic I/F calibration was completed; see Appendix B for a more detailed explanation. Once the images were photometrically corrected, they were each imported into ArcGIS and aligned to their respective locations, using the USGS Europa basemap (USGS, 2002) as reference. The boundaries of potential features were mapped as polygons in ArcGIS. Each feature was then classified into one of seven categories, based on its apparent morphology (Fig. 1).

1. Chaos: a feature with a clear disruption of its interior area, with no clear evidence of topographic changes (i.e. shadows) across the feature, and without evidence of an elevation change within the feature. No distinction is made here between platy chaos and hummocky chaos (Spaun, 2002; Prockter and Schenk, 2005).
2. Dome: a feature with an apparent shadow gradient across it, with the bright side on the sun-facing side, indicating positive topography. While previous work (Greenberg et al., 2003; Singer et al., in review) noted all features that exhibit positive topography, some of them were classified as uplifts, rather than domes, due to their angular shape. Some of these features are included in this data set if it is clear that the uplift is its own independent feature (i.e. distinct from a nearby ridge system). We did not make a distinction between domes and uplifts in the overall analysis done here, but the differences are noted in the data set itself.
3. Pit: an oval- to circle-shaped feature with an apparent shadow gradient across it, with the dark side on the sun-facing side, indicating negative topography.
4. Spot: an enclosed feature with consistent, dark albedo across the entirety of the feature. Presumably the formation of the spot modified the surface to the point where the previous terrain is completely erased because the present spot lacks any obvious signs of further disruption or topography changes.
5. Hybrid: a feature with the typical disrupted interior of chaos that surrounds a topography high or low. Culha and Manga (2017) first identified this microfeature type as dome/chaos, which can appear as hummocky or smooth. Our definition differs from theirs in that we only classified a feature as hybrid if there was clearly a dome/pit inside of the confines of the surrounding chaos, or if a feature appeared to be a dome/pit with a disrupted surface inconsistent with the appearance of the surrounding terrain. Thus, we record two different morphologies for hybrid features (Fig. 1C and D). Note: only dome/chaos hybrids were observed in the study areas, although we cannot rule out the possibility of a pit/chaos hybrid feature outside of our areas of study.
6. Unclassified: a feature with characteristics indicative of a microfeature (e.g., small, round or polygonal, clear delineation from other features) that could not be confidently classified into a specific morphological type at the resolutions available.
7. Crater: a circular feature with negative topographic relief with a well-defined edge (crater rim). This rim is elevated along the entire perimeter of the feature. A central peak may or may not be present, and its absence does not preclude the classification of a crater. Though craters were noted in the data set, they were not included in the analyses as they are formed by an exogenic process, and it is assumed that microfeatures are formed from an endogenic one.

In selecting which quantitative characteristics to extract from our maps, we focused on those that seem to vary between feature types and are easily obtained using native ArcGIS tools. Area and perimeter were calculated with the Shapes and Graphics tool (see below). We used the minimum bounding geometry (MBG) tool to extract the maximum length and maximum width of the smallest rectangle that encloses each feature (Fig. 2), dimensions which we used to calculate the aspect ratio of these rectangles (henceforth called eccentricity): the ratio of the maximum width of a feature divided by its maximum length. Finally, we used the zonal statistics (ZS) tool to retrieve information about the normalized reflectance (the apparent albedo) of each feature. We stress that the normalized reflectance of a feature, while similar to, is not equivalent to a feature's albedo, as it requires photometric corrections that were not performed on the images here due to a lack of photometric constraints for Europa.

The ZS tool notes the digital number (DN) value of each pixel within a feature and calculates a number of metrics about that group of pixels. We recorded only mean, median, standard deviation, and range, though ZS has the ability to output many more metrics. The DNs in this case represent the I/F of the pixel as captured by the *Galileo* SSI camera and corrected using commands in USGS ISIS3 (Anderson et al., 2004); see Appendix B for more information. The final numbers are divided by 65,536, the maximum DN a 16-bit pixel can have, so that all normalized reflectance values are a ratio. A smaller ratio indicates that a feature has a lower overall normalized reflectance (i.e. appears darker). In order to map the entirety of the elliptical domes and pits, parts of the feature that were covered in shadow were also included, lowering the normalized reflectance values for those features. Therefore, the numbers presented here could be considered a minimum value for normalized reflectance. In particular, values for pits and domes may be more representative of the shadows caused by topography than the true albedo of Europa's surface within the feature. Shadowing from topography increases near the terminator, but features are spread throughout the images so there should be no bias towards additional shadowing from topography for any given feature type.

Before extracting data from the images, we applied four sinusoidal projections, one centered on the central meridian of each of the regions studied (Snyder and Voxland, 1994). Table 2 shows the central meridian of each region studied. The sinusoidal projection preserves both shape and size, with the distortion of features increasing with lateral distance from the central meridian, and at high latitudes (poleward of ± 60°) (Snyder and Voxland, 1994). However, as different projections yield different values for area and perimeter, the best measurements are those that are independent of projection. We therefore used the Graphics and Shapes tool (Jenness, 2011), which calculates the true area of polygons and lengths of lines as they lay on the sphere independent of projection. Unfortunately, the tool was not able to calculate the maximum length and width of each polygon, so for those measurements, we used the value computed in the sinusoidal projection. When comparing the areas and perimeters of the features calculated using the sinusoidal projection to those acquired using the Graphics tool, the values were similar to within $< 1\,km^2$ (for area) and < 1 km (for perimeter), and the majority were the same to within half those values. Because of the similarities in the values, and because

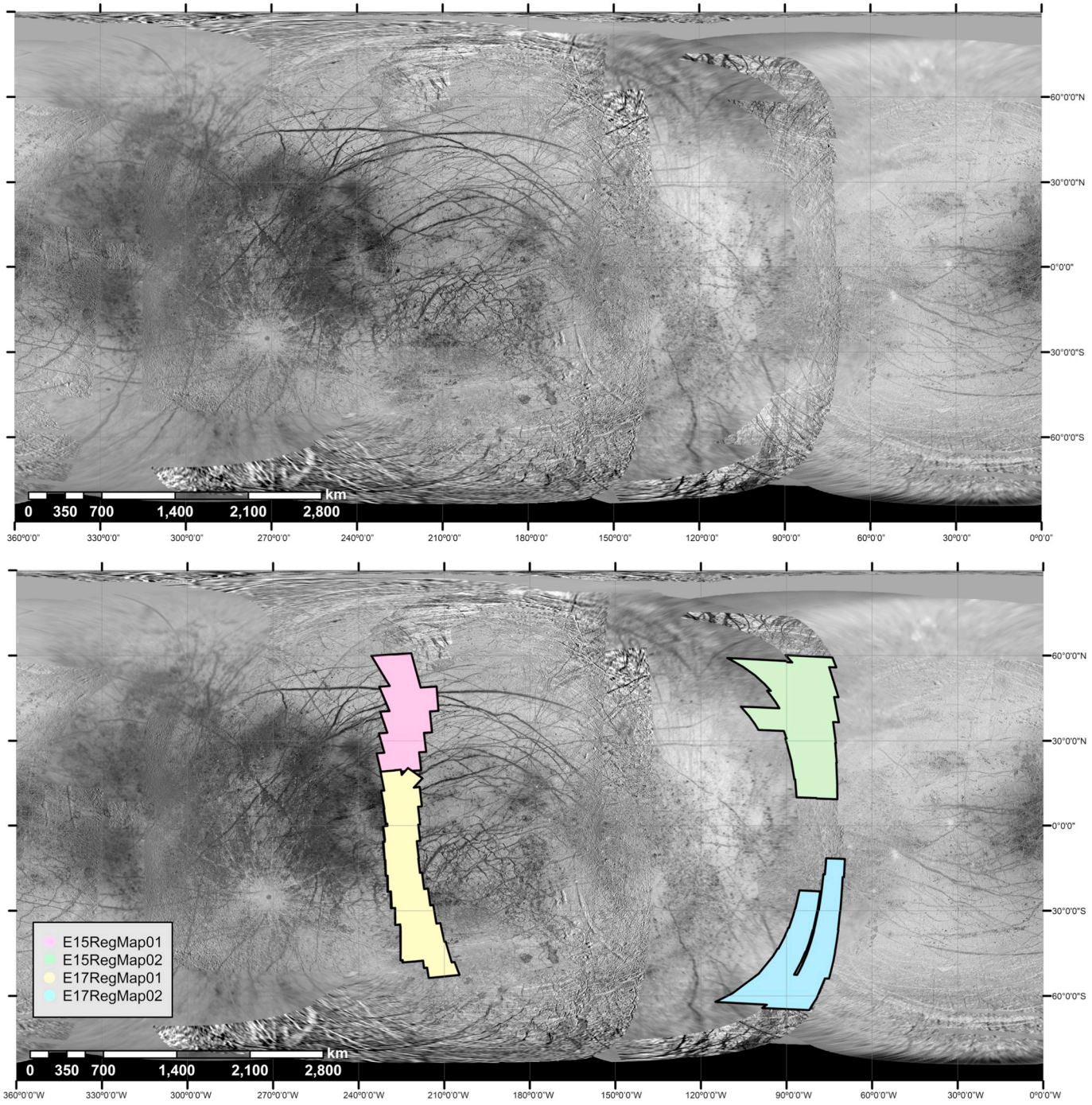

Fig. 2. Global Europa map.
Top: The USGS (2002) basemap of Europa. Bottom: The same basemap with polygons overlain to show our study areas. Pink: E15RegMap01. Green: E15RegMap02. Yellow: E17RegMap01. Blue: E17RegMap02. (For interpretation of the references to color in this figure legend, the reader is referred to the web version of this article.)

Table 2
The central meridians used for the sinusoidal projections in all four RegMaps studied here.

Region	Central meridian mapping longitude
E15RegMap01 (trailing, northern hemisphere)	222°W
E15RegMap02 (leading, northern hemisphere)	83.5°W
E17RegMap01 (trailing, southern hemisphere)	220.7°W
E17RegMap02 (leading, southern hemisphere)	79.5°W

Table 3
Reported measurements for microfeatures ($\leq 100\,km^2$) on Europa in all four RegMaps studied. The asterisk (*) indicates that error could not be estimated due to a small sample size.

Region	Feature type	Total number of features (number excluded based on size cut-off)	Average area (km^2)	Average diameter (km)	Eccentricity (aspect ratio)	Average normalized reflectance
E15RegMap01	Chaos	95 (27)	51.0 ± 2.4	7.9 ± 0.2	0.67 ± 0.03	0.339 ± 0.012
Area: 356,529.51 km^2		Rafts: 11				
	Domes	33 (0)	24.0 ± 2.8	5.2 ± 0.3	0.65 ± 0.04	0.440 ± 0.023
	Hybrids	36 (2)	40.4 ± 3.3	7.0 ± 0.3	0.67 ± 0.02	0.358 ± 0.016
	Pits	119 (0)	29.4 ± 1.6	5.9 ± 0.2	0.67 ± 0.04	0.483 ± 0.011
	Spots	23 (0)	18.8 ± 1.6	4.8 ± 0.2	0.68 ± 0.05	0.278 ± 0.020
	Craters	0	Craters were excluded from analysis			
	Unclassified	33	Unclassified features were excluded from analysis			
	Total analyzed	277				
E15RegMap02	Chaos	209 (120)	43.5 ± 2.5	7.2 ± 0.2	0.68 ± 0.03	0.416 ± 0.011
Area: 613,109.02 km^2		Rafts: 30				
	Domes	30 (0)	14.4 ± 2.0	4.0 ± 0.3	0.63 ± 0.04	0.443 ± 0.020
	Hybrids	25 (1)	35.1 ± 4.1	6.4 ± 0.4	0.65 ± 0.03	0.403 ± 0.019
	Pits	10 (0)	7.5 ± 1.3	3.0 ± 0.3	0.68 ± 0.06	0.486 ± 0.051
	Spots	1 (0)	9.1*	3.4*	0.84*	0.3*
	Craters	7	Craters were excluded from analysis			
	Unclassified	17	Unclassified features were excluded from analysis			
	Total analyzed	154				
E17RegMap01	Chaos	134 (65)	51.7 ± 2.9	7.9 ± 0.2	0.67 ± 0.03	0.377 ± 0.012
Area: 630,229.91 km^2		Rafts: 21				
	Domes	33 (1)	18.1 ± 3.0	4.4 ± 0.3	0.72 ± 0.03	0.417 ± 0.019
	Hybrids	23 (1)	36.4 ± 4.9	6.5 ± 0.4	0.64 ± 0.03	0.385 ± 0.018
	Pits	21 (0)	21.1 ± 3.6	4.8 ± 0.4	0.70 ± 0.04	0.402 ± 0.026
	Spots	4 (0)	10.7 ± 3.6	3.5 ± 0.6	0.60 ± 0.03	0.448 ± 0.023
	Craters	1	Craters were excluded from analysis			
	Unclassified	2	Unclassified features were excluded from analysis			
	Total analyzed	148				
E17RegMap02	Chaos	13 (0)	47.3 ± 8.1	7.4 ± 0.7	0.69 ± 0.05	0.318 ± 0.026
Area: 490,409.50 km^2		Rafts: 0				
	Domes	21 (0)	19.5 ± 2.2	4.8 ± 0.3	0.75 ± 0.03	0.398 ± 0.029
	Hybrids	10 (0)	35.1 ± 5.4	6.5 ± 0.5	0.68 ± 0.07	0.340 ± 0.037
	Pits	67 (0)	17.5 ± 1.4	4.5 ± 0.2	0.66 ± 0.02	0.387 ± 0.014
	Spots	1 (0)	6.7*	2.9*	0.50*	0.07*
	Craters	13	Craters were excluded from analysis			
	Unclassified	43	Unclassified features were excluded from analysis			
	Total analyzed	112				

only those two measurements could not be acquired with the Graphics tool, we felt confident using the few measurements that are projection-dependent.

2.2. Validating the data set

To ensure accuracy in our classifications of mapped features, we compared our maps with three other data sets (Greenberg et al., 2003; Culha and Manga, 2017; Singer et al., in review), which required that we first digitize the data set collected by Greenberg et al. (2003). In general, the features that were included in the final analysis were those that were mapped in at least two out of the four datasets, allowing for exceptions if a feature is clearly present but only included in any one of the four data sets. The reason for this level of validation is primarily to account for the advance in technology that occurred between the creations of different data sets, and to allow for the maximum number of verified features to be counted in the final tally. The largest difference between the data sets is the number of features. Some data sets completely omitted features that at least two others included. The oldest data set (Greenberg et al., 2003) was most prone to this. Another reason for omission of features between data sets is that different data sets mapped in slightly different areas. For example, even if all data sets included the same RegMap, there were some areas within the RegMap where only two data sets overlapped. It was not clear if the other data sets failed to map features because they were outside of a predetermined study range, or if the creators did not see any features there. There were also some features that are clearly present, but extend beyond the RegMap images. We excluded such features from our data set on the basis that we could not retrieve complete information about those features within images of the same resolution. Finally, Greenberg et al. (2003) did not include spots and chaos in their data set, so those feature types could only be compared between three data sets overall. Singer et al. (in review) included spots as a separate category, but they were analyzed as part of the chaos group because they were so few in number. Similarly, the only two data sets that included “hybrids” as a category were ours and the Culha and Manga (2017) data set, though our definitions of a hybrid feature are different. As a result, some flexibility was built-in to accommodate the differences in the data sets.

The second difference between data sets lay in determining the boundaries of the features. The largest variation existed in the chaos features, especially in both RegMap02 regions, where there are multiple large chaos features—larger than the area covered by the RegMap images—that intersect the RegMap. Chaos features are irregularly shaped, and it is not clear in some cases where the boundary of one chaos feature ends and another begins. In these cases, only chaos features that were clearly distinct from one another were mapped in our data set. This led to some chaos features being omitted. The chaos feature sizes and shapes also varied between data sets, as the boundaries themselves were often inconsistent between data sets, especially between that of ours and Culha and Manga's (2017). In those cases, we chose to include the polygon from our data set for consistency. Because we digitized the Greenberg et al. (2003) data set, the features are not exactly the same shape and size as the authors originally mapped them, though we tried to remain as true to the original as possible. In some cases, it was unclear what feature they mapped, and therefore some of their features (~5% of the total) were omitted from the digitization. For the most

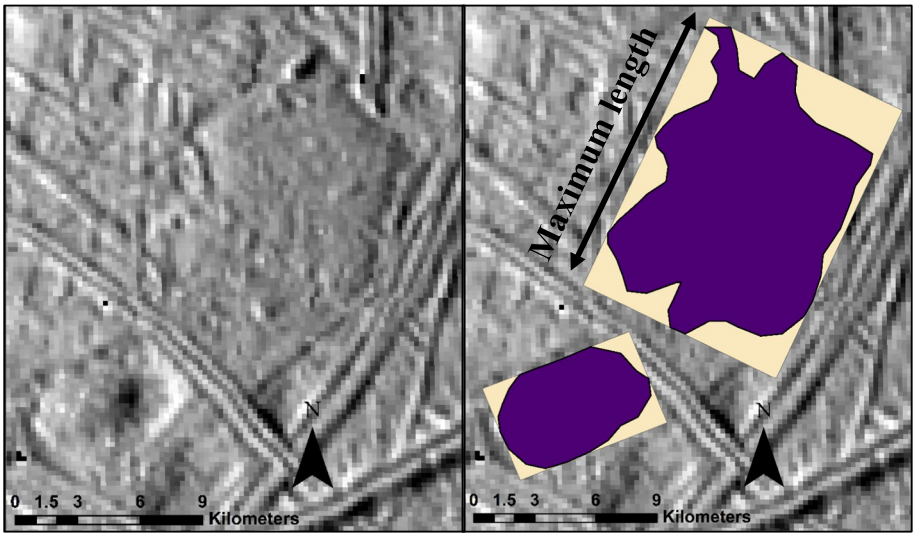

Fig. 3. Maximum length.
FID #52 and 53 in E15RegMap02. Some polygons drawn in ArcGIS overlying the rectangles created by the minimum bounding geometry (MBG) tool. The maximum length of a feature is defined as the length of the rectangle. Sun angle is from the top.

part, pits and domes were consistent in shape and size across data sets, as were spots when they were noted. Slight variations existed in orientation of the pits and domes, but the overall location was consistent across datasets.

Once the final data set was validated, we removed all features larger than 100 km^2 in area, which is equivalent to a circle with a diameter of 11.2 km. This size cut-off was chosen to narrow the data set to a size range that was applicable to all microfeatures in order to explore the relationship between feature types. Because we focus on this smaller size range, we collectively refer to the pits, spots, domes, hybrids, and small chaos features in our study as microfeatures. This term is based on the fact that these features look small in the images of Europa that are currently available. We do note that the Europa Clipper mission will return images with resolutions better than 50 m/pix over 95% of the surface (Turtle et al., 2016; Bayer et al., 2018), at least four times better than the resolution of the images used here. The higher resolution images may reveal even smaller features that were not visible in the currently available images; therefore, the term "microfeature" is likely a temporary one.

Finally, after validating the data sets and setting the size range, we determined the characteristics of the data. In the context of statistics, the sample refers to the features mapped in this study, which represent a subset of the entire population of features. For each characteristic we quantified, we computed an "error" that estimates the expected amount of variation in the measurements within each microfeature group. To calculate error we used the standard error (SE) equation of $SE = \frac{\sigma}{\sqrt{N-1}}$, where σ is the sample standard deviation of the data and N is the total number of features being analyzed. The factor of $\frac{1}{\sqrt{N-1}}$ converts the sample standard deviation into the unbiased estimate of the true population standard deviation from the available sample.

We report here (Table 3) the overall number of features of each type in each RegMap, and the average areas, diameters, eccentricities, and

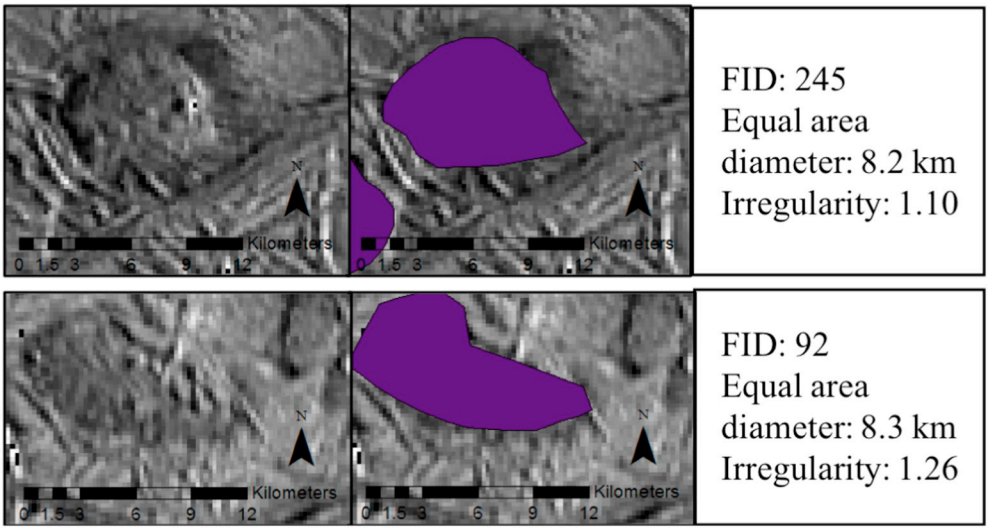

Fig. 4. Irregularity.
Visualization of the irregularity measurement using two features from E15RegMap01. These two features have the same equal area diameter, but their different shapes mean they have very different irregularity measurements. These features are both chaos, illustrating some of the variety of chaos feature shapes.

normalized reflectances of each of these feature types. We also include how many features were excluded from the study as a result of the size cut-off, and to what category they belonged. In the case of chaos, we note how many contained any evidence of rafts. We also include information on the maximum lengths of these features overall (Fig. 3), as this may be the measurement used to determine average feature sizes in previous studies (Carr et al., 1998; Greeley et al., 1998; Pappalardo et al., 1998, 1999; Spaun, 2002).

We also developed a method to quantify the shapes of microfeatures, specifically a feature's irregularity. Qualitatively speaking, chaos features in particular tend to have irregular shapes whereas other microfeature types are more elliptical. We initially calculated the diameter of a circle of equal area, represented by the equation: $Diam. = 2 * \sqrt{\frac{Area}{\pi}}$, for each microfeature as a way to consistently speak about the size of the feature. This information is used again to calculate the circumference of an equal-area circle. We then divide a feature's perimeter by the equal-area circle circumference. This will yield a ratio with a minimum value of 1.0, indicative of a perfect circle. A feature with a higher perimeter-to-circumference ratio will be more irregularly shaped (Fig. 4).

3. Results

3.1. E15RegMap01, northern trailing hemisphere

All four data sets included features in this region (Fig. 5). There are 306 total verified microfeatures in E15RegMap01 (Table 3). We excluded 27 chaos features and two hybrid features because they exceeded the size limit of 100 km^2, leaving 277 features in our data set (Fig. 5). The most numerous feature type was pits (119), followed by chaos (68); domes, hybrids, and spots were less numerous and had similar numbers of features (33, 34, and 23, respectively) (Fig. 6). Chaos and hybrid features in this region are significantly larger than the domes, pits, and spots, which are all around the same size in both area and diameter. The eccentricities of all microfeature types do not differ significantly. Out of all 68 microchaos features mapped, 11 (16%) had evidence of rafts, but all features only had one or two, and the resolution of the images made it difficult to resolve any details about them (Fig. 7).

In this region, the spots have the lowest mean normalized reflectance (i.e. they appear darker), followed by chaos and hybrids. Pits and domes have significantly higher normalized reflectance values than chaos, spots, and hybrids, making them appear brighter overall, although the reflectance values are affected by shadows and brightening related to their topography. As one side of pits and domes is directly illuminated, while chaos, hybrids, and spots are generally flat, the observation that pits and domes are brighter is consistent lighting and imaging geometries of the images. Pits and domes do differ significantly from each other in terms of normalized reflectance, with pits having the higher normalized reflectance.

3.2. E15RegMap02, northern leading hemisphere

All four studies mapped in this region, but each study had slightly different boundaries, resulting in some areas where our data set only overlapped with one other. There are 282 total verified features in E15RegMap02 (Fig. 6), including craters, with 154 that are < 100 km^2 (Table 3), fewer than were in E15RegMap01. Chaos features are by far the most numerous feature type in this region (89), with similar, smaller numbers of domes and hybrids (30 and 24, respectively). In stark contrast to E15RegMap01, there were only 10 pits and 1 spot identified in this region, and 7 craters. This region sits within what appears to be a larger platy chaos region that extends well beyond the limits of the RegMap (Riley et al., 2000; Leonard et al., 2017; Leonard et al., 2018), which may contribute to the high number of features that are over 100 km^2. Chaos formation destroys preexisting terrain, so the presence of a large zone of chaos likely contributed to the overall lower numbers of identifiable microfeatures in this region. The eccentricities of all microfeature types do not differ significantly in this region either. Out of all the microchaos features mapped, 30 (34%) of them had evidence of rafts.

The chaos features are significantly affected by the size cut-off; 120 chaos features and one hybrid feature were removed when the size cut-off was imposed. Even below the size cut-off, chaos and hybrids are on average larger than the domes, pits, and spots, which are all around the same size in both area and diameter. This is consistent with the results in E15RegMap01. Pits in this region are 2 to 4 times smaller, on average, than pits in all other regions. The feature types with the lowest normalized reflectance values are spots, hybrids, and chaos features, with pits and domes both significantly brighter, and pits having the highest normalized reflectance.

3.3. E17RegMap01, southern trailing hemisphere

All four studies mapped in this region, but not all mapped down to the same latitude. There are 216 total verified features in this region (Fig. 7), including one crater, and 149 of these are < 100 km^2 (Table 3). Chaos features are the most numerous (69), with about half as many domes (32) and a third as many pits and hybrids mapped and validated (22 and 21, respectively). Of the features that exceeded the size limit, all but two were chaos. One of the remaining features belonged to the hybrid class, and one was a particularly large uplift, the only one over 100 km^2 in any of the four mapped regions. Once again, the chaos and hybrid features are significantly larger than the domes and pits, which are all around the same size in both area and diameter, consistent with the results from other regions. The spots (4 in total) are significantly smaller in area and diameter than any other feature type, another consistent result across the regions. The domes and pits in this region also have an eccentricity that is significantly different from chaos, hybrids, and spots. Spots have a significantly lower eccentricity than all other microfeatures. Out of all microchaos features mapped, 21 (30%) had evidence of rafts.

The normalized reflectance of chaos is the lowest of all the features, followed by hybrids. Domes and pits are around the same normalized reflectance value, though domes are slightly brighter. This could indicate that the pits in this region are deeper than in other regions, and their large shadows are lowering the overall mean normalized reflectance values. According to these values, the spots have the highest normalized reflectance in this region, but this could be due to a small sample size, which is associated with higher errors.

3.4. E17RegMap02, southern leading hemisphere

In this region, there are significantly fewer features than in any other, and they are consistently smaller than in the other regions (Fig. 8). Out of the 125 total features in E17RegMap02, only one – a crater - was excluded based on size (Table 3). This region also had the most overall number of craters (13). Pits are the most numerous features (67), and there are a third as many domes (21). In general, all features are significantly less numerous than in any other region. Domes outnumber both chaos and hybrid features (13 and 10, respectively), the only region where this is observed. The chaos and hybrid features are significantly larger than the domes, pits, and spots, which are all around the same size in both area and diameter. The eccentricities of chaos and hybrids do not differ significantly to any other feature type, but the eccentricities of domes and pits are significantly different from each other. Out of all microchaos features, none had clear evidence of rafting. Chaos features, and one spot, are the darkest features in this region, and hybrid features are slightly brighter than chaos. Domes and pits are, on average, the brightest feature types in this region.

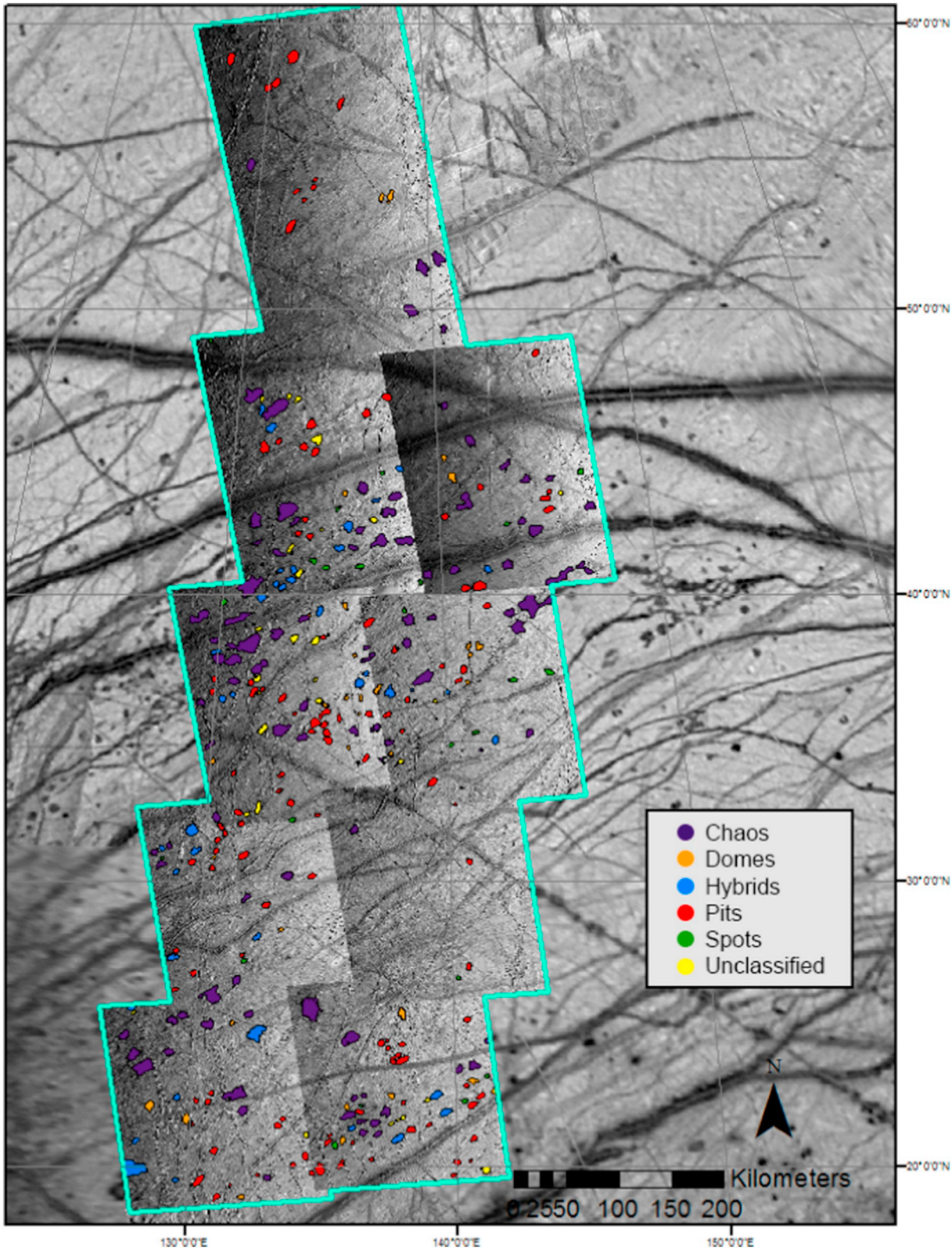

Fig. 5. E15RegMap01.
E15RegMap01, with mapped features shown as polygons. Purple polygons are chaos. Orange polygons are domes. Blue polygons are hybrids. Red polygons are pits. Green polygons are spots. Yellow polygons are potential features that were mapped, but left unclassified. No craters were observed in this region. (For interpretation of the references to color in this figure legend, the reader is referred to the web version of this article.)

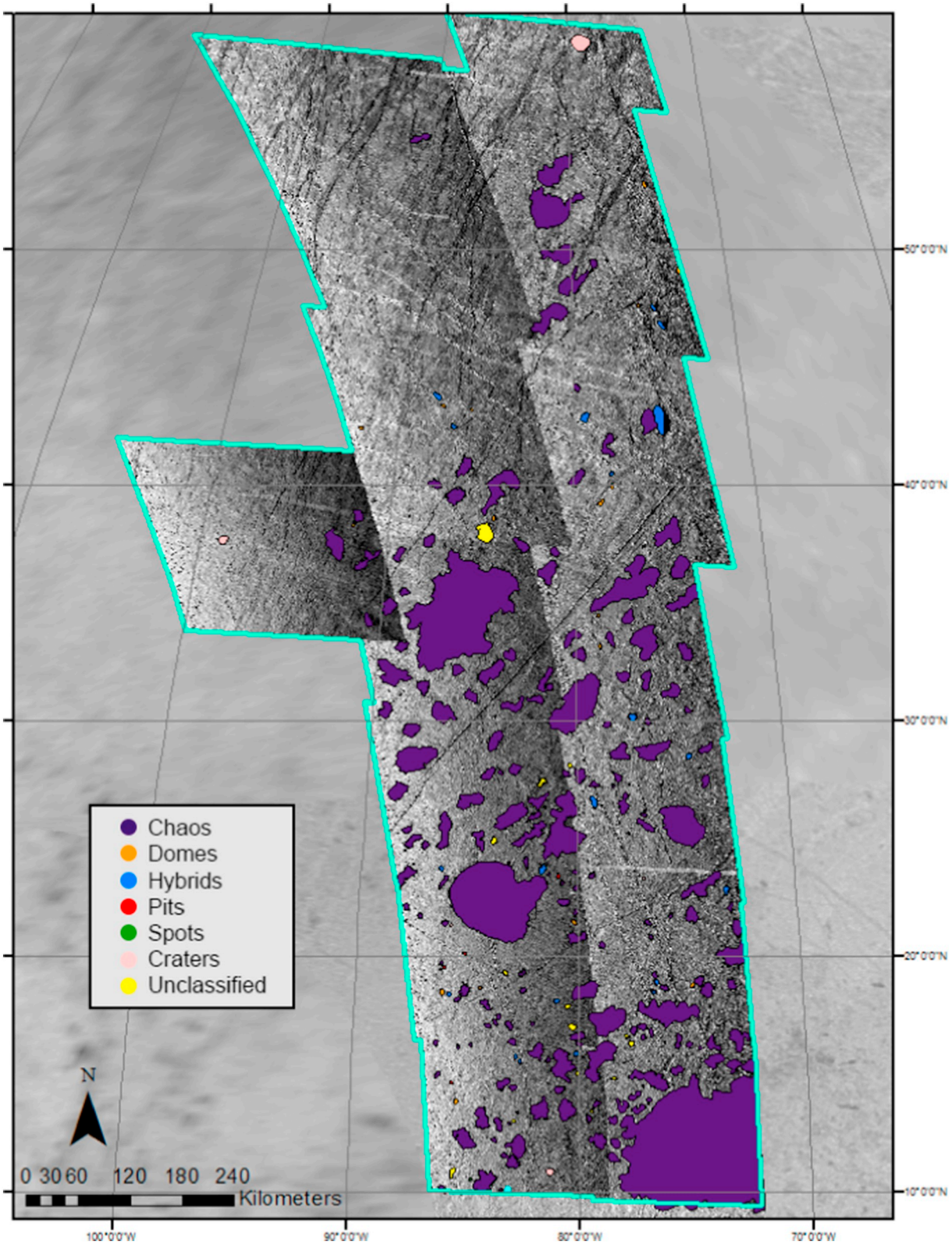

Fig. 6. E15RegMap02.
E15RegMap02, with mapped features shown as polygons. Purple polygons are chaos. Orange polygons are domes. Blue polygons are hybrids. Red polygons are pits. Green polygons are spots. Pink polygons are craters. Yellow polygons are potential features that were mapped, but left unclassified. (For interpretation of the references to color in this figure legend, the reader is referred to the web version of this article.)

a) Top

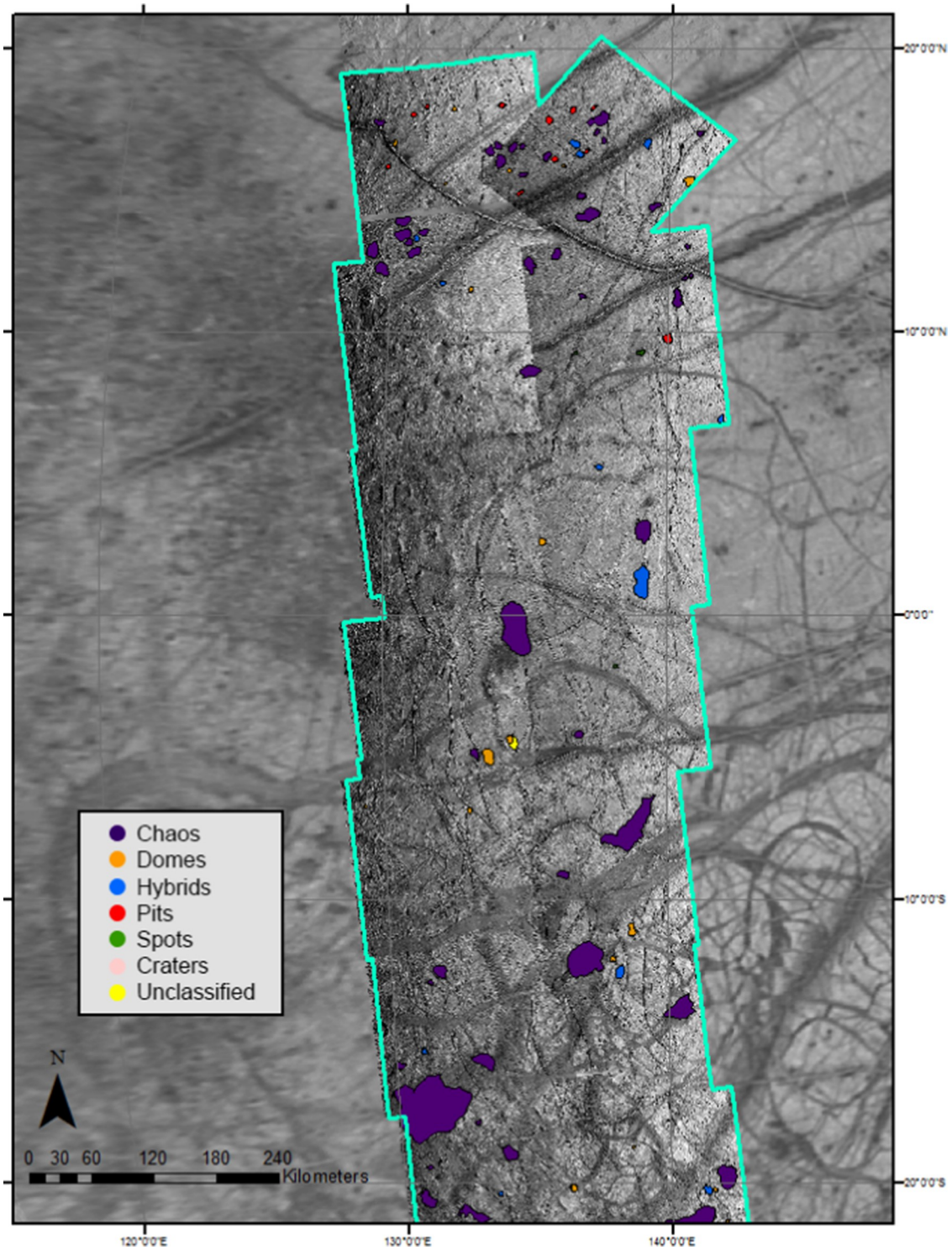

Fig. 7. E17RegMap01.
A: The top section of E17RegMap01, with mapped features shown as polygons. Purple polygons are chaos. Orange polygons are domes. Blue polygons are hybrids. Red polygons are pits. Green polygons are spots. Pink polygons are craters. Yellow polygons are potential features that were mapped, but left unclassified.
B: The bottom section of E17RegMap01, with mapped features shown as polygons. Purple polygons are chaos. Orange polygons are domes. Blue polygons are hybrids. Red polygons are pits. Green polygons are spots. Pink polygons are craters. Yellow polygons are potential features that were mapped, but left unclassified. (For interpretation of the references to color in this figure legend, the reader is referred to the web version of this article.)

b) Bottom

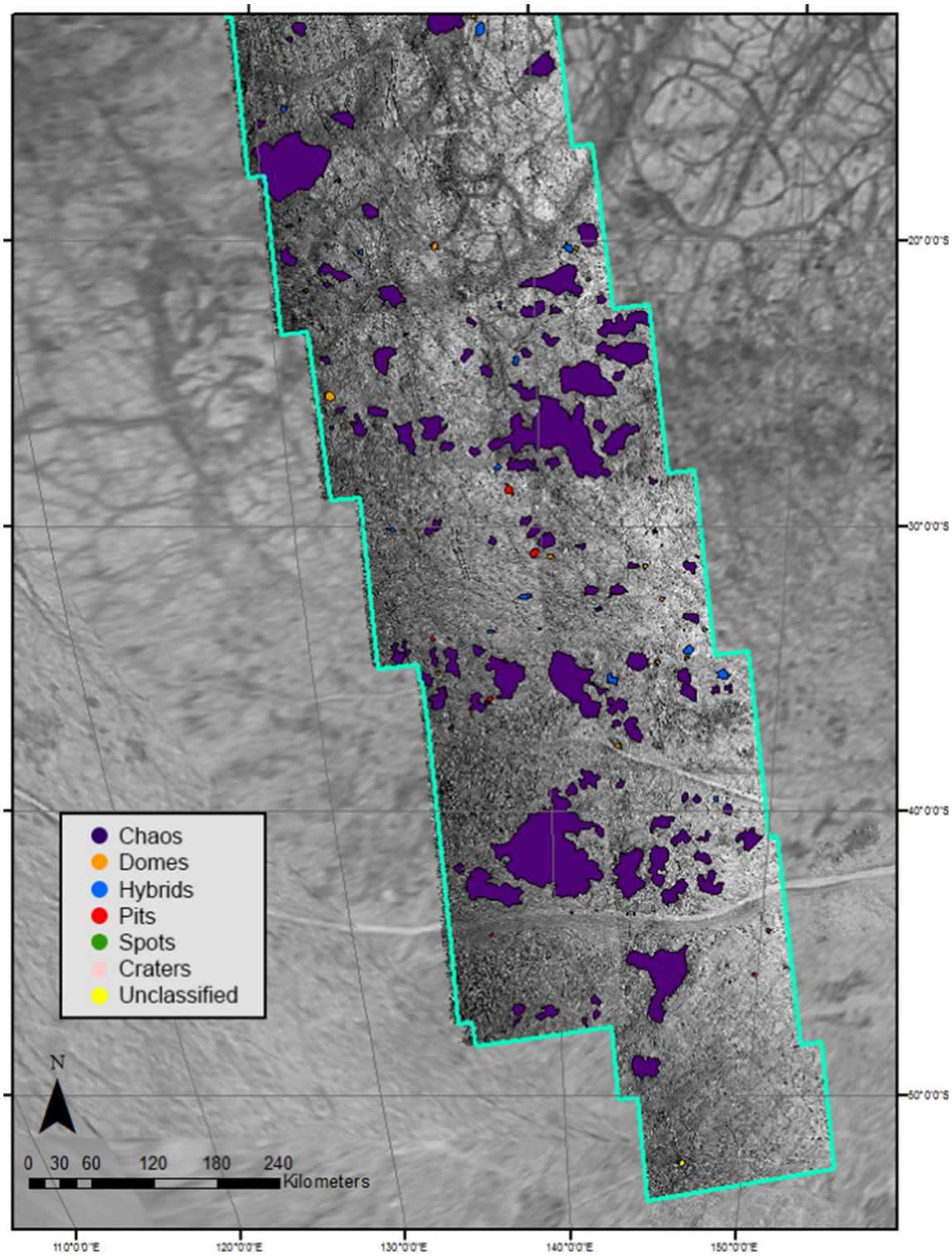

Fig. 7. (*continued*)

3.5. Overall observations

Comparing across all four mapped regions (Table 4), chaos is the most numerous feature, almost equaled in number by pits. However, chaos features are more consistently numerous whereas pits are spatially heterogenous. Spots are the least common, overall, and most spots are concentrated in one region (E15RegMap01). Domes are most consistent in terms of their spatial distributions, with roughly equal numbers in all regions, even those with lower numbers of total features.

In the area histogram (Fig. 9) the bins represent 5 km^2 in area. The data points on the histogram represent the centers of the bins. Chaos and hybrid features are significantly larger than the domes, pits, and

a) Top

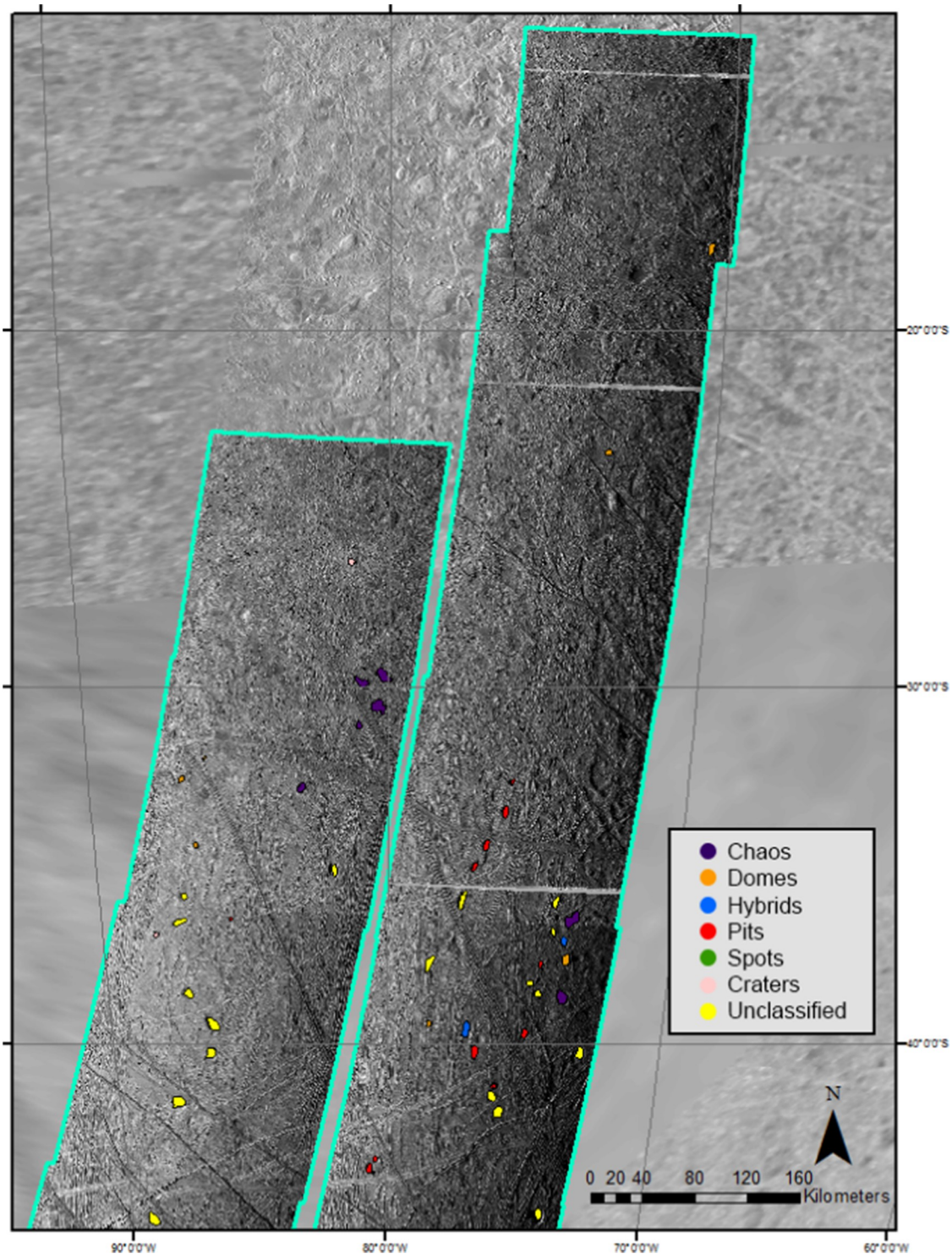

Fig. 8. E17RegMap02.
A: The top section of E17RegMap02, with mapped features shown as polygons. Purple polygons are chaos. Orange polygons are domes. Blue polygons are hybrids. Red polygons are pits. Green polygons are spots. Pink polygons are craters. Yellow polygons are potential features that were mapped, but left unclassified.
B: The bottom section of E17RegMap02, with mapped features shown as polygons. Purple polygons are chaos. Orange polygons are domes. Blue polygons are hybrids. Red polygons are pits. Green polygons are spots. Pink polygons are craters. Yellow polygons are potential features that were mapped, but left unclassified. (For interpretation of the references to color in this figure legend, the reader is referred to the web version of this article.)

b) Bottom

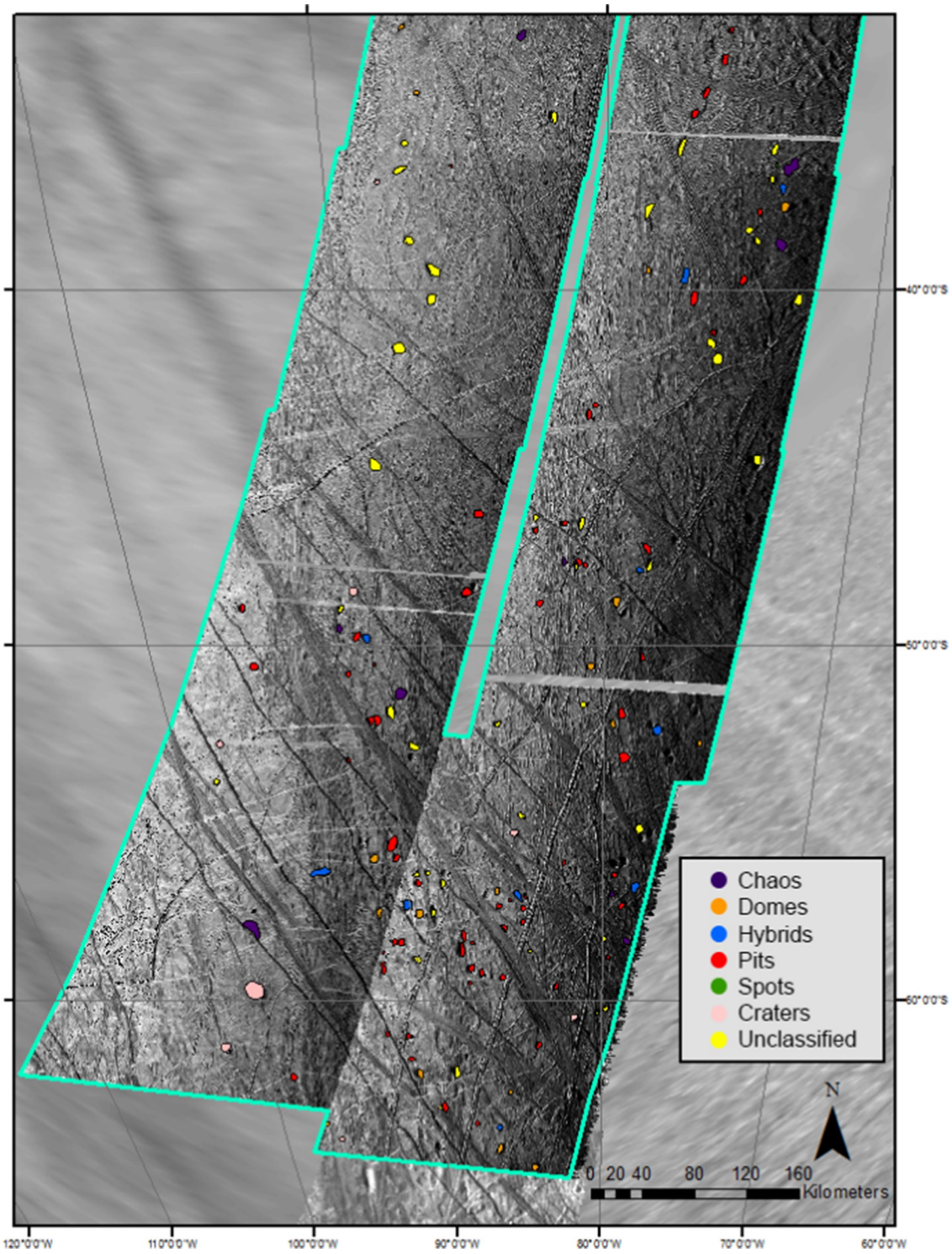

Fig. 8. (*continued*)

spots, which are all around the same size in both area and diameter. The size distribution of pits and domes both indicate a higher concentration of features at smaller sizes, but no features under 1 km can be confidently measured due to the resolution limit. The size distribution of spots is also clustered at small sizes; it both ascends to and descends from its peak more gradually, and there are no spots larger than 35 km^2. Pits have a definite peak between 10 and 15 km^2, while domes have a broader peak between 5 and 25 km^2. Hybrids have a small peak around 25 km^2, but above this size the distribution is uniform until it gradually drops off at larger sizes. Chaos dominates in number at large areas, though there is at least one pit and one hybrid feature that reach at least 90 km^2 in area (excluding the dome that was removed due to size cut-off constraints in E17RegMap01). Chaos has a roughly normal distribution, with a clear peak between 50 and 60 km^2. The rise up to the peak is roughly linear, and after the peak the counts remain approximately uniform until the upper size limit of 100 km^2. There is an

Table 4
Global numbers. The hybrid types are broken down into more detail in this chart, but are not individually their own microfeature classification.

Feature type	Number of features	Average area (km^2)	Average diameter (km)	Eccentricity	Average normalized reflectance	Average irregularity
Chaos	239	48.2 ± 1.5	7.6 ± 1.5	0.68 ± 0.04	0.377 ± 0.007	1.16 ± 0.01
Domes	116	19.1 ± 1.3	4.6 ± 0.2	0.68 ± 0.06	0.427 ± 0.011	1.10 ± 0.01
Hybrids (all)	90	37.5 ± 2.1	6.7 ± 0.2	0.66 ± 0.04	0.374 ± 0.010	1.12 ± 0.01
Hybrids: Type I	*23*	*38.8 ± 5.1*	*6.7 ± 0.5*	*0.65 ± 0.11*	*0.369 ± 0.021*	*1.15 ± 0.02*
Hybrids: Type II	*67*	*37.0 ± 2.2*	*6.7 ± 0.2*	*0.66 ± 0.07*	*0.376 ± 0.022*	*1.11 ± 0.01*
Pits	217	23.9 ± 1.1	5.2 ± 0.1	0.67 ± 0.05	0.445 ± 0.010	1.10 ± 0.01
Spots	29	16.9 ± 1.5	4.5 ± 0.2	0.67 ± 0.06	0.295 ± 0.021	1.13 ± 0.02
Total	691					

Total area studied: 2,090,277.94 km^2 (6.43% of Europa's surface area).
The italicized text represents the more detailed specifics of the Type I and Type II hybrid.

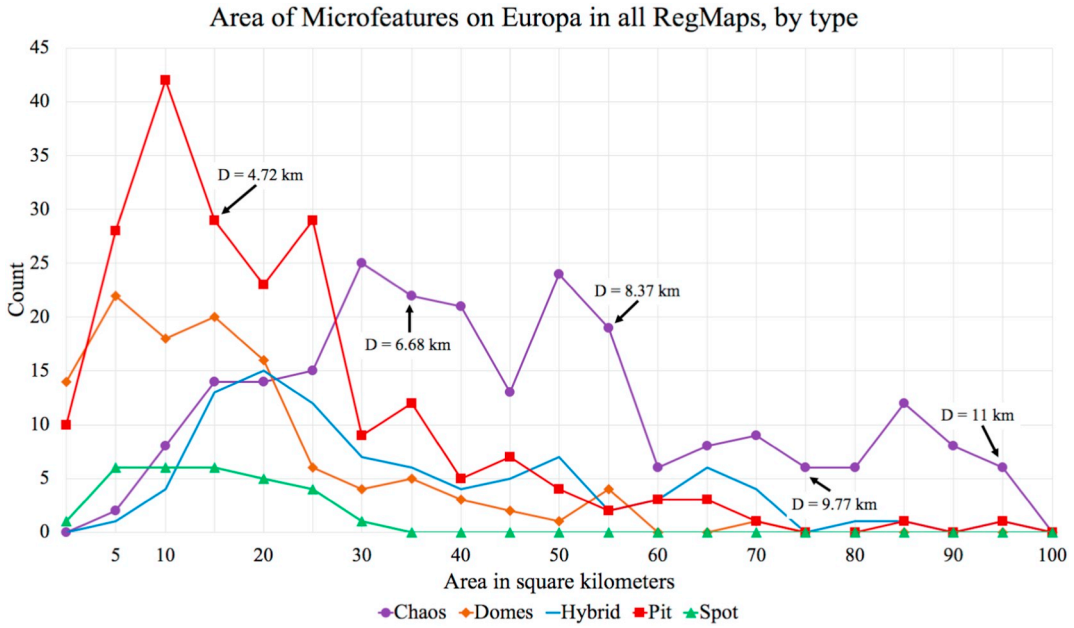

Fig. 9. A line histogram showing the areas of microfeatures in the four RegMaps studied here, separated by type. Bin sizes are consistent throughout the chart and represent areas of 5 km^2.

imposed truncation in the chaos distribution due to the size cut-off at 100 km^2, which is expected as chaos features are known to exist above the size cut-off. All other feature types decline in number at large sizes and are, therefore, unaffected by our imposed size limit. We also observe a steep drop off in the number of features below a few km^2, which may be a resolution effect (see also, discussion in Section 4.1). A similar size distribution was reported by Singer et al. (in review).

We also examined maximum lengths of features. The maximum length of a feature is likely to be larger than the equal area diameter as a feature can be eccentric or shaped irregularly (Fig. 10). The equal area circle diameter does not retain information related to how a feature is shaped, but the maximum length is more sensitive to these differences. Maximum length is also an easier measurement to envision, and previous studies may have considered the lengths of these features while describing their sizes. Like the areas, the majority of the features of all types cluster around small sizes. Pits and domes peak between 4 and 7 km in maximum length, while hybrids and spots peak between 5 and 7 km. Only chaos features peak around 10 km, a "typical size" reported in past studies (e.g., Pappalardo et al., 1998; Riley et al., 2000; Spaun, 2002; Collins and Nimmo, 2009; see discussion in Section 4.2), though it is noted that only small chaos was considered in this study. Even so, these peaks are broader than those seen in the area histogram, implying a broad range of sizes.

Overall, spots are the darkest features, although they are also the least numerous features, which makes them susceptible to large errors due to a small sample size. In all four study areas, chaos and hybrids have around the same normalized reflectance values, although chaos is slightly darker. This shared characteristic suggests a common process affecting the formation of chaos, spots, and hybrid features. Domes and pits have roughly the same values of normalized reflectance, with pits being slightly brighter than domes. The higher normalized reflectance of pits may be due to their geometry; there is more area within pits that reflects sunlight, which is both a function of their topography (i.e. the depth and symmetry of an individual pit) and the lighting angle of the image. An asymmetrical pit may have one side that reflects more sunlight than the other, while a non-nadir lighting angle could increase the amount of the sunlight in the pit. In E15RegMap02, the normalized reflectance values are higher on average than in the other regions, indicating that this region was more illuminated than other regions were, which resulted in a brighter set of images even after photometric correction. It could also increase the length of a dome's shadow, another reason for why the dome's average normalized reflectance value is slightly lower than that of pits.

3.6. Locations of microfeatures

In order to compare the number of features below and above the equator, we broke down the data set into these two latitudinal groups, regardless of the RegMap in which a feature was mapped. There are more than twice as many features above the equator than below it (482

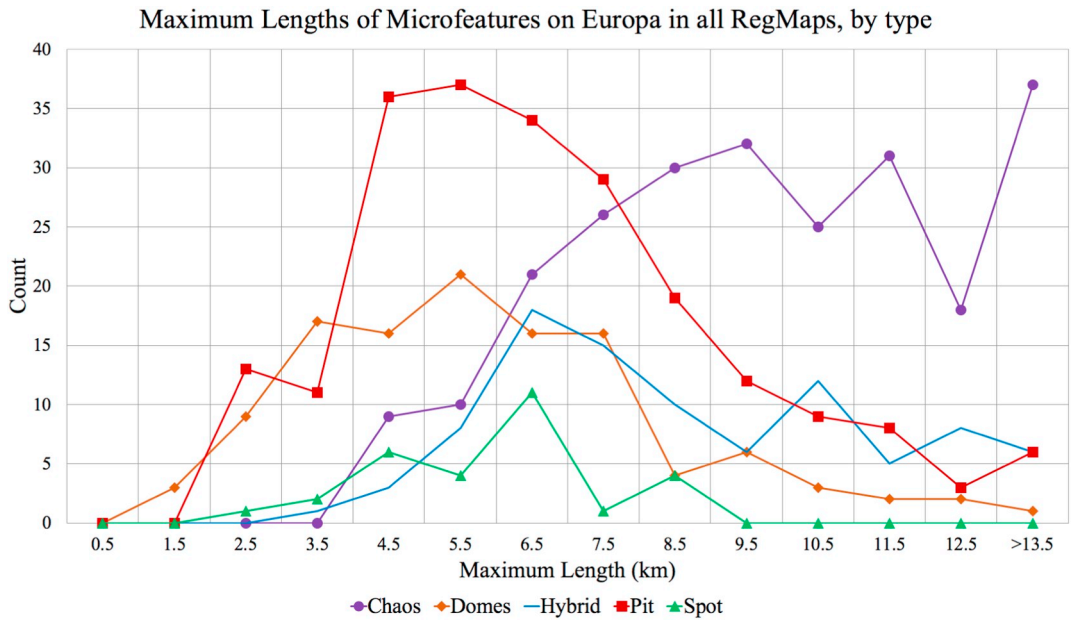

Fig. 10. Line histogram of max lengths for all feature types in all RegMaps.
A line histogram showing the maximum lengths of microfeatures in the four RegMaps studied here, separated by type. The points represent the center of the bin. Bins are the same size and represent distances of 1 km in length.

features above compared to 211 below), even though the total area mapped in the southern hemisphere was larger than the total area mapped in the northern hemisphere. We did the same with longitude and compared the number of features in the leading hemisphere to the number in the trailing hemisphere. Once again, there was a large discrepancy in the number of features between the two hemispheres; there are 425 features in the trailing hemisphere, and 266 in the leading hemisphere. The total area mapped in the trailing hemisphere is smaller than the total area mapped in the leading hemisphere. We discuss possible reasons for these population size differences in Section 4.1.

3.7. Eccentricity and irregularity of features

Overall, eccentricities do not vary between microfeature types, though this does not hold true for each region. Domes and pits had the smallest irregularity measurement of all the features. Chaos has the highest average irregularity of all the feature types, which is significantly higher than pits, domes, and hybrids. Spots have a high irregularity value, but with a small data set, the error is high. These results are consistent with the qualitative result that chaos is irregularly shaped. It also suggests that the average irregularity of chaos features is significantly different from that of domes and pits. Hybrid features have an intermediate average irregularity value, but are more similar to the average domes and pit irregularity values overall.

3.8. Hybrids

In simplest terms, hybrids are a blend between a chaos feature and a dome, but not all hybrid features combine chaos and domes in the same ratio. What we have defined as Type I hybrid morphology shows an elliptical, topographically-positive feature within a dark “moat” that is usually smoother than the surrounding terrain. This “moat” can be smooth or hummocky, similar to the interiors of some chaos features. The domes and uplifts within these hybrid features usually have a disrupted surface, though it is not true of every case, and are smaller than the full extent of the “moat.” The Type II hybrid morphology shows a dome or an uplift with a significantly disrupted surface, and lacks the “moat” characteristic of the Type I hybrids. While some domes retain the evidence of a cross-cutting ridge or trough, the Type II hybrid features show a disruption pattern that is inconsistent with the surrounding terrain. These features have been noted previously in the literature; Greenberg et al. (2003) described these kinds of features as cracked domes, and their varying morphologies have been noted in other papers (Fagents, 2003; Quick and Marsh, 2016; Quick et al., 2017).

Overall, there are 67 Type II hybrids and 23 Type I hybrids, a ratio of about 3:1. The only region where Type I hybrids outnumber Type II hybrids is E17RegMap01. In all regions, there is no significant difference in size between the two hybrid types; indeed, the equivalent diameter for both types is identical. There is also no significant difference in the eccentricities of the two hybrid types. The Type I hybrid features have a significantly lower average normalized reflectance than the Type II hybrids, as the “moats” are dark and exhibit little variation in topography or albedo, as opposed to the dome-like Type II hybrid features. Type I hybrid features also have higher irregularity than the Type II hybrid features, and share a value more similar to that of chaos.

4. Discussion

In this study, we merged four data sets of microfeatures in Europa's four RegMap areas to create the most robust data set possible. The shape files are available in an online supplement. In total, we mapped, validated, and characterized 691 microfeatures across Europa's surface. These observations are presented as constraints for present and future modeling efforts.

4.1. Implications of microfeatures characteristics

Small chaos features and pits are the most numerous types of microfeatures across the four regions studied, although pits are spatially heterogeneous whereas chaos is more consistently prevalent across all regions. Pits are sometimes numerous even in regions that have fewer microfeatures overall, making up anywhere from 6% to 54% of the microfeatures in a given region. In contrast, the number of domes and hybrids are relatively uniform across all four regions, and spots are always much less prevalent than other microfeature types.

To further explore spatial differences in the number and character of microfeatures, we must first consider potential sources of observational

bias. First, there is an extensive area of dispersed chaotic terrain in the leading hemisphere between ~10°N and ~30°S (as mapped by e.g., Riley et al., 2000), which reduces the mappable area in E15Regmap02 and E17Regmap01. No individual microfeatures could be confidently mapped within this broad region of surface disruption, which could partially explain why we identified fewer microfeatures in the southern hemisphere and the leading hemisphere, and the fewest in the south leading hemisphere (E17RegMap02). In addition, the presence of many large chaos features, which we mapped but excluded from our reported feature counts, were much more numerous in the north leading hemisphere than in other regions. The presence of these larger features leaves less area in which to identify microfeatures, so they may also contribute to the smaller number of features observed in the leading hemisphere. Therefore, the relative numbers of observed microfeatures may be more suggestive of a difference in the character of chaos features, from clusters of microchaos to discrete large chaos features to diffuse regions of disruption, across Europa's surface.

Separate from the issues of observational bias, there appears to be a spatial difference in the character of chaos features. While microfeatures are more concentrated in the northern and trailing hemispheres, large chaos features are more numerous in the leading hemisphere, especially in the E15RegMap02 area (Riley et al., 2000; Leonard et al., 2017). From previous mapping studies (Riley et al., 2000; Figueredo and Greeley, 2004; Collins and Nimmo, 2009; Culha and Manga, 2016; Leonard et al., 2017), the largest chaos features are mapped close to Europa's equator, including Conamara and Manannán. The largest chaos features mapped in this study were in the E15RegMap02 and E17RegMap01 regions, which are in the northern, leading quadrant and southern, trailing quadrants, respectively. Thera and Thrace Maculae lie in between the two southern RegMaps studied here, but they are more fully situated in the trailing hemisphere.

It is interesting that the quadrants with the larger features are diagonal to each other, which may point to a symmetric heating source driving the formation of these larger chaos features. Part of the reason for this could be attributed to differences in the ice shell properties in these regions; if fractures penetrate deeper where tidal stresses are larger, sills could form in higher numbers or with different depths and sizes that contribute to the prevalence of larger chaos. It could also be that there is a concentration of heat at low-latitudes on Europa, perhaps as a result of latitudinal heterogeneity (Soderlund et al., 2014), and this heat creates the larger chaos features. Concentrations of large chaos features have been previously noted (e.g., Schenck et al., 2008) near 120°W and 300°W in support of a polar wander scenario, which could be interpreted to support diapirism, as tidal heating is most concentrated near the poles (Collins and Nimmo, 2009). While there appear to be no obvious correlations between the locations of large chaos patches to predictions regarding the equilibrium ice thickness (e.g., Ojakangas and Stevenson, 1989), the limited spatial extent of this mapping project makes it difficult to address and characterize global processes that could drive microfeature formation, and an extensive modeling project addressing these issues is outside the scope of this manuscript.

The morphology of chaos features may also suggest a difference in the formation process between large and small-scale features. Chaos has two different, well-documented morphologies: platy (e.g., Conamara chaos) and hummocky (e.g., Murias chaos). Roughly 41% of the surface area of Conamara chaos is platy (Spaun et al., 1998), a typical value among larger chaos features (Spaun, 2002). We identified some clear examples of platy chaos at smaller sizes ($< 100\,km^2$) within the regional mapping data set, a result consistent with the identification of individual rafts within some smaller chaos features around Conamara (Tognetti et al., 2017; Leonard et al., 2018). Even when potential rafts were found, however, they were not numerous and it was difficult to note any details about them, a result also reported in Leonard et al., 2018. The lack of discernable rafts within small chaos features could potentially be a result of image resolution, or it could point to a difference in the way surface disruption occurs during the formation of large and small-scale chaos features. The fact that rafts in small-scale features have been identified in proximity to the archetypical example of platy chaos (i.e. Conamara) may also suggest that microchaos can develop as part of the formation of large-scale features, with morphologies dictated by the formation process of the large features.

In the model of Manga and Michaut (2017), pits form as an intermediate phase of microfeature formation in which liquid water is present within the ice shell. That model implies that the differences in pit density in different regions represents a heterogeneity in the presence of liquid water within the shell, perhaps suggesting that regions with fewer pits have not experienced recent endogenic activity. We note that the region with the fewest pits (E15RegMap02) also has the largest number of craters, lending credence to the idea that the surface is older, with less endogenic activity in the recent past than other regions. Although that region is affected by the presence of large chaos features potentially reducing the area in which features can be identified, the decline in the number of pits relative to other regions is much more drastic than for other feature types.

We found no evidence to support past assertions that microfeatures have a typical diameter of 10 km (Carr et al., 1998; Greeley et al., 1998; Pappalardo et al., 1998; Spaun, 2002). Instead, we find that microfeature types vary in their typical sizes, each type presents over a fairly wide range of sizes, and only chaos features display any size characteristics consistent with typical diameter of 10 km. Chaos and hybrid features are significantly larger than pits, domes, and spots across all regions studied. The average sizes of domes and pits are within each other's error bars. Even when considering the maximum lengths of the features, only chaos features peaked around 10 km, while all other features peaked at significantly smaller sizes. A better estimate for the average size of microfeatures of all types is 2–6 km in terms of equal area diameter, and 4–9 km in terms of maximum lengths.

Because the pixel scale of the images was at least 218 m/pix, and assuming a five-pixel detection limit, the smallest feature that could be confidently identified in this study is ~1 km in diameter, as reported by Singer et al. (in review). The rapid decrease in number of features we observe as area drops below roughly $10\,km^2$ could indicate that there is a minimum size associated with the formation of microfeatures, but the detection limit within the regional mapping images may also play a role. Singer et al. (2010) looked for pits and domes in the limited set of higher resolution images across Europa, including ones that cover parts of the RegMaps, and did not find features of increasingly smaller size. We caution that even though the results of Singer et al. (2010) and this study are consistent, this team has only looked at roughly 7% of Europa's total surface, and smaller features could exist outside of these areas studied.

Many previous chaos mapping studies (Head and Pappalardo, 1999; Greenberg et al., 1999; Prockter et al., 1999; Spaun et al., 1999; Greeley et al., 2000; Riley et al., 2000; Spaun, 2002; Figueredo et al., 2002; Greenberg et al., 2003; Figueredo and Greeley, 2004; Spaun et al., 2004; Collins and Nimmo, 2009; Schmidt et al., 2011; Culha and Manga, 2017; Leonard et al., 2017) note that chaos features typically have low albedo, although there are counterexamples (e.g., Conamara chaos). A higher albedo does not exclude a feature from being classified as chaos, and instead introduces a new dimension to understanding chaos and its relation to other microfeatures. We find that chaos, spots, and hybrid features have similar normalized reflectance values, which may support the claim that their formation involves a similar process. We also find that their normalized reflectances are lower than those of pits and domes. We can make comparisons within our data set because the imaging geometry is similar and we have applied the same photometric corrections of all of the images. The normalized reflectance

values may not be the same in images with different imaging geometries or lighting conditions, and the normalized reflectances we report may not be well-correlated with albedo.

Lower albedo terrain on Europa is usually associated with reddish-brown material, which has been interpreted as evidence of salts on Europa's surface (McCord et al., 2002; Dalton et al., 2005; Carlson et al., 2005; Carlson et al., 2009; Hand and Carlson, 2015). Brine inclusion has been suggested as a feature of chaos formation (Head and Pappalardo, 1999; Han and Showman, 2005) because the inclusion of salts and other impurities will lower the melting temperature of ice, making it easier for surface disruption to occur. The fact that domes and pits have higher average normalized reflectances than chaos, hybrids, and spots may imply that briny, liquid water is only brought to the surface during the formation of the latter features. However, we cannot rule out the idea that liquid water in the shallow subsurface plays a role in the formation of pits and domes, as in the model of Michaut and Manga (2014), particularly because normalized reflectance is dependent on photometric correction and viewing geometry, and thus, may not be an accurate indicator of lower albedo material.

The source of liquid water within the ice shell is still undetermined. Liquid could form as partial melt at the top of a rising diapir within a convecting ice shell, or ocean water could be injected into the ice shell by an overpressurized ocean through a pre-existing fracture in the ice. Work by Hand and Carlson (2015) shows that the reddish-brown color is more consistent with sodium chloride irradiated over long periods of time in Europa's environment, and argues that it is evidence that Europa's ocean is in direct contact with the surface. This interpretation is more consistent with the liquid water sill hypothesis (Schmidt et al., 2011; Michaut and Manga, 2014; Manga and Michaut, 2017) than with the in situ partial melt one. Still, the possibility that the salts are hydrated sulfate salts (McCord et al., 2002; Dalton et al., 2005) or sulfuric acid hydrate (Carlson et al., 2005) cannot be ruled out.

4.2. Predictions associated with formation models

Multiple studies (Pappalardo et al., 1998; Rathbun et al., 1998; Pappalardo and Barr, 2004; Collins and Nimmo, 2009, and references therein; Schmidt et al., 2011; Culha and Manga, 2016; Manga and Michaut, 2017) have suggested that all of these microfeature types are related. They could be different stages of one process occurring on Europa, or the same process yielding different results because of the particular environment in a certain location. We now compare our observations with the predictions and assumptions of the main formation models: diapirism, cryovolcanism, and sill formation.

Pappalardo et al. (1998) first suggested that the different microfeatures are genetically related, and that domes and chaos were especially indicative of a warm-ice diapir within a convecting ice shell between 3 and 10 km thick. One piece of evidence in favor of this model was that the microfeatures appeared to be around the same size, between 7 and 15 km in diameter, in an area centered at 15°N and 270°W (Conamara region). This region is not included in our data set. We find that, broadly speaking, microfeatures are similarly sized, but most features are smaller than the range reported by Pappalardo et al. (1998), and that chaos features are substantially larger than other feature types. Hence, if all microfeatures are formed though diapirism, the diapirs would need to be capable of producing smaller surface features (e.g., 4–7 km across), consistent with the sizes we observed outside the Conamara region.

Rathbun et al. (1998) studied 42 domes in the same region. Their findings corroborated the diapirism model in that the features were a consistent size, but they noted a potential problem: diapirs small enough to have formed the observed domes would have lost their heat too quickly, even before they reached the surface. Hence, while small diapirs could explain the presence of small isolated domes, the domes should be rare. Rathbun et al. (1998) also noted that some of the domes had surrounding "moats," which is more consistent with our definition of hybrids than domes. We find that domes and hybrids are roughly half as numerous than microchaos and pits, but they are much more common than spots.

Later work examined the roles that concentrated tidal heating (Sotin et al., 2002; Mitri and Showman, 2008; Han and Showman, 2010), plasticity of the ice shell (Showman and Han, 2005), and salinity (Pappalardo and Barr, 2004; Han and Showman, 2005) have on the ability of a diapir in a convecting ice shell to produce the observed microfeatures. In general, these papers focused primarily on chaos and dome formation, and only one explicitly mentioned the formation of pits (Showman and Han, 2004). None addressed the formation of spots. Han and Showman (2005) used numerical simulations to show that a diapir with sufficient temperature and salinity contrast to the surrounding ice would become buoyant enough to form uplifts and pits with 100–500 m of relief, consistent with later mapping results (Schenk and Pappalardo, 2004; Singer et al., 2010; Singer et al., in review). However, they were unable to create features with the diameters observed here; all their features were between 10 and 30 km in diameter (78.5 km^2 and 706.9 km^2 in area, respectively), almost exclusively outside of the range examined here. While there are chaos features in this size range, there are almost no domes and pits that are those sizes. Furthermore, in a later study, they were unable to produce any isolated pits or uplifts/domes of any diameter (Showman and Han, 2005), which is inconsistent with our observations. Based on the current modeling results, the small sizes and prevalence of pits and domes are inconsistent with the diapir formation model. However, because chaos features and hybrids are typically larger than other microfeature types, we cannot rule out diapirism as a formation mechanism for chaos.

Quick and Marsh (2016) investigated whether the cracked domes (called Type II hybrid features here) could have been formed by cryovolcanism. They used numerical simulations to first verify that cryomagma can ascend within Europa's ice shell. They found that warm ice can move through Europa's lithosphere, and that its speed is comparable to ascent velocities of terrestrial magma diapirs moving through Earth's mantle (Quick and Marsh, 2016). On Earth, dikes and pre-existing fractures can be used repeatedly by multiple magma ascensions, eventually forming features such as shield volcanoes. A similar process could happen on Europa, and domes could be the result of repeated eruptions of cryolava on the surface (Quick and Marsh, 2016). Later work on dome relaxation revealed that the model dome topographic profiles match the estimated dome heights observed on Europa. Moreover, they found that the average dome radius is 3 km, consistent with our observations (Quick et al., 2017). They also investigated the compositional evolution of the cryomagma inside of a diapir, as an eruption could bring material to the surface from Europa's interior, and provided more evidence that the salts observed on Europa's surface are endogenic (Quick and Marsh, 2016). Cryovolcanism is consistent with the sizes of domes and hybrid features, and it provides a natural explanation for the lower normalized reflectance of hybrid features. However, this model does not provide a natural mechanism for forming chaos features, pits, or spots, which would suggest multiple processes or different manifestations of cryovolcanism in order to explain all microfeature types. Additionally, no evidence of flow features was observed.

The microfeature formation model proposed by Manga and Michaut (2017) invokes the presence of a liquid water sill, in which the depth of the sill relative to the surface and the strength of the ice layer containing the sill control whether a dome or a pit is formed. A sill that forms at a shallower depth will have more support from the ice beneath it, allowing it to expand upwards and outwards, increasing the positive

relief of the overlying ice and the lateral extent of the feature itself. This arrangement will form a dome. A sill that forms deeper in the ice shell, near the boundary between brittle and ductile ice layers, will not have the bottom support to grow, so it will instead become deeper, with a lesser lateral extent. This negatively warps the surface above the sill, forming a pit. However, the evolutionary stage of the sill and the radius of the sill itself can affect the appearance and size of the feature it potentially creates; as the liquid water freezes, the model predicts that pits will evolve into domes. Hence, pits could indicate pockets of deeper liquid water whereas domes could indicate shallow liquid water or frozen sills that initially created pits.

This model also predicts that domes should be larger than pits (Manga and Michaut, 2017). The model first relates the depth of the sill to the size of the feature. If there exist two sills at the same depth in the ice shell where, due to differences in the depth of the elastic layer of Europa's ice shell, one sill formed a dome and the other formed a pit, then the dome should have a larger diameter despite the same sill depth. This is because the weight of the liquid water in the sill will cause the ice underneath the sill to warp downward, causing "the intrusion's lateral extent [to] decrease a few tens of percent" (Manga and Michaut, 2017). We find that pits and domes are not significantly different in either average overall area or average diameter, which disagrees with the model prediction. Additionally, the model suggests that larger water bodies are more likely to lead to disaggregation of the surface, forming chaos features. Because larger sills form larger surface features, chaos features should be larger on average than the other microfeature types. Our results are consistent with this prediction. Chaos is, on average, larger than domes and pits, implying that the sills that form chaos are larger than sills that form pits and domes. Smaller chaos features may be formed from a single sill or a combination of a couple of small sills, while larger chaos (e.g., Thrace Macula) may be formed from many sills merging together to form a sill complex, or via a separate process altogether. The ratio between blocky and hummocky chaos at various sizes could provide more clues to the formation of chaos features.

The sill model (Manga and Michaut, 2017) also supplies a continuum of microfeature formation involving the evolution of liquid water pockets within Europa's ice shell. The model states that chaos and domes are both end-stage microfeature types, and both pits and domes can form as an intermediate stage. Assuming the process takes less time than Europa's surface age, the most numerous feature type is most likely to represent the end stage of this continuum process. Therefore, our results would imply that microchaos is the most common end stage, as it outnumbers all other features. It could also be that it is easier to create microchaos from domes than Manga and Michaut (2017) suggest. If the shallow water sills create domes that crack while the liquid water is freezing (effectively overpressurizing the sill itself), fractures would be created on the dome's surface, which could be the origin of the cracked dome Type II hybrid feature. The overpressures in the freezing sill could also lead to the remaining liquid to escape through the fractures, where it could become the low-albedo material seen around the Type I hybrid features and within the matrix of microchaos (Manga and Michaut, 2017).

Careful attention should be paid to hybrid features in general. Their classification has evolved from domes with "moats" (Rathbun et al., 1998; Quick et al., 2017) and cracked domes (Pappalardo and Barr, 2004; Greenberg et al., 2003) to an independent feature type (Culha and Manga, 2016; this study). The range of hybrid morphologies and the fact that hybrid features exhibit similarities to both chaos and domes support the idea that they are intermediate features between domes and small chaos. According to the Manga and Michaut (2017) model, domes may turn into chaos features, and hybrids could represent this transition. Hybrids are similar in number to domes, and have intermediate sizes between domes and chaos features. The presence of two different morphologies also supports this idea. The formation ideas from the previous paragraph could apply, but they are not the only explanations for hybrids. The Type I hybrid features with their dark "moats" could reflect the progressive cracking of the surface from the outside in, as would happen as the sill freezes and overpressure increases. This explains why the dome in the center is often disrupted as well, as the surface would have been affected at an earlier stage as the sill was growing. Cryovolcanism cannot be ruled out either, especially in the formation of hybrids and domes, as the "moats" could be interpreted as the surface's response to an effusion of cryolava (Quick et al., 2017). Without more information, it is difficult to say for sure which formation mechanism is more likely.

Both pits and domes are supposed to form as intermediate features, while the weight of the liquid water sill warps the surface before it later freezes. However, pits are almost as numerous as small chaos features, whereas domes are only half as numerous as microchaos or pits. Hence, our results suggest that domes are not the most common end state and calls into question the hypothesis that domes would form during multiple phases of microfeature evolution. Instead, our results support the idea that the formation of pits, and not domes, is the more-commonly taken route between an unaltered surface and the conclusion of microfeature emplacement, likely as a chaos feature. Alternatively, it is also possible that the domes that would form from the sills underneath current pits simply have not frozen yet to form the domes, suggesting that microfeature formation is relatively recent.

This begs the question of why there are fewer domes than expected, relative to chaos and pits. Domes are predicted to form as an intermediate stage of microfeature evolution when a sill in emplaced higher in the ice shell (Manga and Michaut, 2017). It is more challenging to get large volumes of water to a higher level in the ice shell, which means that it would be harder to form domes than pits. Domes are also hypothesized to form when the sill freezes, even if the surface expression of the sill had been a pit during the liquid phase. Hence, some pits may have turned into domes. Therefore, we might expect a correlation between older surfaces (i.e., those less affected by recent endogenic activity) and higher numbers of domes relative to pits. In any case, the reduced number of domes compared to chaos and pits must be fully explained by any formation model.

One observation that could shed more light on the relationship between hybrids, domes, and chaos features is the potential change in the numbers of features in the same regions studied here once Europa Clipper returns data from Europa in the mid- to late-2020s. If the number of hybrids relative to domes has increased, then it could mean that domes are changing into hybrid features. Recalculating the ratio between Type I and Type II hybrid features could also be telling. First we assume that if the microfeatures form along a continuum, then the end stage feature type should be the most numerous. If there are more Type I hybrids relative to Type II hybrids or vice versa in the future, it could be interpreted as evidence for the progression of microfeature formation, and for the direction of formation (i.e., do domes turn into chaos or does chaos turn into domes?). If the ratio remains roughly the same, it could mean that there is no continuum, or that these features form at the same rate.

4.3. Implications for formation of microfeatures

We have identified several key characteristics of microfeatures, some of which have not been previously noted in the literature, that can serve as constraints for future modeling efforts.

1. Chaos and hybrid features are larger than pits, spots, and domes. Chaos is the only microfeature that presents at scales larger than

100 km^2, and the peak size is larger than that of domes and pits. This indicates that whatever process creates chaos and hybrids typically affects a larger area on Europa's surface during their formation. The relative sizes of different feature types may indicate that disruption events are more likely to occur for larger features. One hypothesis, presented by Manga and Michaut (2017), is that the merging of multiple sills would weaken the overlying ice, leading to the cracked and hummocky surfaces characteristic of chaos and hybrid features. However, any formation model would also need to explain smaller chaos features and the domes that form within Type I hybrids.

2. Chaos is the most common type of microfeature, and the second most common is pits. The relatively high frequency of chaos features may indicate that chaos formation is the most likely end state in a progression of microfeature formation, as suggested by Manga and Michaut (2017), or that conditions for chaos formation are more readily met than for other feature types. A future model needs to explain why chaos is more common than other features, and why pits are more numerous than domes, which is counter to the prediction of Manga and Michaut (2017). The relative ages of different regions – with high pit density indicative of more recent endogenic activity – could potentially account for the larger number of pits relative to domes. However, the region that had the highest number of craters, E17RegMap02, had the fewest overall features but the second highest number of pits, so the relationship between crater-based age and the presence of liquid water within the shell is not obvious.
3. Chaos and hybrid features are irregularly shaped. We have quantified the irregularity of microfeatures and found that pits, spots, and domes are generally more elliptical in nature (though they can be polygonal), while chaos and hybrid features often have irregular shapes and wavy perimeters, even if they are not bounded by a ridge system. Merging sills (e.g., Manga and Michaut, 2017) could be useful in explaining this observation. Multiple ellipsoidal-shaped sills could merge to make an irregular surface expression, depending on their sizes, depths in the ice shell, and relative orientations. Furthermore, microchaos features are far more likely to have hummocky, rather than platy, interiors.
4. Hybrid features come in two distinct types. What we have termed Type I hybrids have a dome surrounded by a dark “moat,” which presents as hummocky chaos. In this case, the majority of the domes inside of the hybrids show a disrupted surface themselves, indicating that the dome is simply raised from the previous chaotic terrain. This interpretation implies that the domes are younger than the chaos feature, although the domes may have formed in direct response to chaos formation. Type II hybrids present as domes with severely disrupted surfaces, which have higher normalized reflectance than the Type I hybrids. Because features tend to darken over time when exposed to radiation (Hand and Carlson, 2015), the fact that these Type II hybrids are not as dark as Type I hybrids or chaos suggests that the Type II hybrids could be younger than the Type I hybrids. Another possibility is that Type II hybrids have simply not experienced any surface rupture that allowed material to flow over the surface, since that is the material that would darken over time.
5. Spots are the rarest and smallest of all microfeature types. Spots also have consistently low normalized reflectance value across all four RegMaps, similar to chaos features and hybrids, perhaps indicating a common process that occurs in the formation of all three types. Previous models (Schmidt et al., 2011; Manga and Michaut, 2017) have posited that spots are formed when the surface is minimally disrupted after the spot is formed, such that it remains mostly flat. An alternative hypothesis is that spots are the result of surface disruption but that the scale of the event is below the resolution limit of currently available images. In that case, spots are simply small chaos features whose interiors have not been fully resolved, rather than a distinct feature type.

5. Conclusion

In an effort to understand the underlying process or processes that govern microfeature formation on Europa, we mapped all visible microfeatures in the E15RegMap01, E15RegMap02, E17RegMap01, and E17RegMap02 regions. We classified these microfeatures into chaos, domes, hybrids, pits, spots, or left them unclassified; we also noted craters, where present. We used data sets from other studies (Greenberg et al., 2003; Culha and Manga, 2016; Singer et al., in review) to validate our features and ensure high robustness and accuracy of the final feature database. Our results show that chaos and hybrids are larger than all other microfeature types, while pits and domes are around the same size, and spots are the smallest overall. Pits and domes are smaller than the “typical” size reported in past studies (Greenberg et al., 2003; Culha and Manga, 2016). Chaos is the most numerous microfeature, followed by pits, then domes, then hybrids, and finally, spots. The average normalized reflectance values of chaos, spots, and hybrid features are significantly lower than pits and domes, consistent across all regions studied. We also found that there are more microfeatures in the northern hemisphere than the southern, and more in the trailing hemisphere than the leading one, although the presence of large chaos features may be introducing an observational bias.

We have compared our results to predictions made by some microfeature formation models. Diapirsm may explain microchaos and domes, but the predicted sizes of these features are larger than the observed sizes, and numerical models of diapirism have not reproduced pits and spots. Extrusive expressions of cryovolcanism on Europa (Quick et al., 2017) may explain the formation of domes, as their predicted heights and radii match the profiles of those domes produced by the model. Unfortunately, this model does not yet explain pits, spots, or microchaos, and is presently only supported by observations of domes, equivalent to diapirism. Finally, a sill model (Manga and Michaut, 2017) explains the presence of all microfeature types as part of the sill's evolution, including the presence of hybrids as a transitional feature type, and can explain the overall numbers and sizes of microfeatures observed. However, the large number of pits relative to domes in some areas suggests that regional characteristics may exert some control on whether domes form or that some regions may have experienced less endogenic in the recent past than others. From these observations, the cryovolcanism and sill models are most consistent with our results.

Future mapping work should address whether or not microfeatures can occur on Europa at sizes smaller than 1 km in diameter and the degree of clustering of microfeatures on Europa. Mapping efforts can also be expanded to areas that were not included in this study, with particular attention paid to the appearance and morphology of hybrid features and the addition of normalized reflectance measurements. This data set will serve as the basis of future geophysical and statistical modeling efforts, which will inform future mission planning including both the upcoming Europa Clipper and potential future lander missions.

Acknowledgements

We would like to thank Moses Milazzo, Cynthia Phillips, Alfred McEwen, and Vishaal Singh for their help photometrically correcting the images of Europa used here. We'd also like to thank our reviewers, Erin Leonard, Alex Pathoff, and Francis Nimmo for their thoughtful and detailed comments. This work was supported by NASA's COLDTech and SSW programs, grants NNX17AF70G and NNX15AH91G, respectively.

Appendix A. All images used in the analysis

E15RegMap01

Image ID	Incidence angle	Emission angle	Phase angle	Pixel resolution	Center longitude (360 W)
1800r	80.77	27.42	62.79	231.58	229.16
1814r	80.77	27.42	62.79	231.58	228.01
1827r	80.00	32.49	62.91	231.69	226.62
1840r	79.63	38.82	63.04	232.12	225.86
1852r	79.87	46.48	63.17	232.97	224.88
1865r	81.15	55.96	63.29	234.39	222.08
1879r	74.47	24.29	63.10	228.46	220.47
1901r	74.47	24.29	63.10	228.46	218.62
1914	73.81	30.30	63.22	228.64	216.69

E15RegMap02

Image ID	Incidence angle	Emission angle	Phase angle	Pixel resolution	Center longitude (360 W)
4252r	21.76	81.75	232.23	232.30	77.40
4265r	28.22	75.09	233.49	233.58	84.41
4278r	26.16	81.60	233.79	233.87	77.88
4300r	32.07	74.87	235.09	235.19	85.38
4313r	31.74	81.57	235.59	235.69	78.68
4326r	37.10	74.72	236.93	237.06	86.17
4339r	38.31	81.45	237.68	237.80	79.03
4352r	43.34	74.58	239.09	239.26	87.69
4365r/4366r*	45.30	82.46	240.00	240.17	78.52
4378r	49.90	75.48	241.45	241.69	88.88
4401r	100.24	54.69	82.36	243.31	80.45
4413r	100.68	59.65	75.16	245.20	93.46
4426r	100.16	67.05	82.32	248.90	82.27
4439r	101.22	50.21	68.70	243.96	97.64

E17RegMap01

Image ID	Incidence angle	Emission angle	Phase angle	Pixel resolution	Center longitude (360 W)
4152r/4153r*	81.27	28.67	71.31	227.98	228.12
4165r/4166r*	81.28	22.37	71.23	226.75	227.81
4178r/4179r*	74.78	20.72	71.67	226.07	221.31
4200r/4201r*	75.35	14.20	71.56	225.06	222.15
4213r/4214*	75.49	8.54	71.51	224.25	222.03
4226r/4227r*	76.39	5.09	71.41	223.63	222.31
4253r/4254r*	76.41	7.16	71.38	222.65	221.58
4265r/4266r*	75.83	12.02	71.41	222.36	220.43
4278r/4279r*	74.85	17.69	71.50	222.23	218.26
4300r/4301r*	74.50	23.95	71.55	222.32	216.47
4313r/4314r*	74.23	31.07	71.63	222.62	213.92
4326r/4327r*	75.07	38.34	71.64	223.22	212.49
4340r	75.97	46.68	71.68	224.16	210.37
4500r[&]	77.91	25.78	100.15	202.63	222.21
4552r	80.73	17.37	70.63	212.45	227.47
4565r	81.17	13.24	70.54	211.66	227.68
4578r	81.51	11.23	70.48	211.05	227.65
4600r	81.37	11.60	70.47	210.56	227.03
4613r	81.00	14.34	70.49	210.21	226.01
4626r	80.40	18.66	70.55	210.01	224.73
4639r	79.82	23.77	70.61	209.99	223.20
4652r	79.09	29.64	70.71	210.17	221.08
4665r	80.16	36.44	70.67	210.61	220.65

& = taken on E19 orbit of the Galileo mission.

E17RegMap02

Image ID	Incidence angle	Emission angle	Phase angle	Pixel resolution	Center longitude (360 W)
6752r	83.22	12.27	91.81	217.87	72.92
6778r	83.25	17.44	91.85	219.23	73.99
6800r	77.32	26.79	92.28	220.66	82.38
6813r	83.29	23.54	91.88	220.81	74.50
6826r/6827r[a]	77.24	33.11	92.32	222.50	84.05
6839r	83.29	30.32	91.92	222.63	75.51
6852r/6853r[a]	77.16	40.28	92.35	224.65	86.20
6865r	83.24	37.77	91.95	224.74	76.79
6878r/6879r[a]	76.95	48.79	92.39	227.24	90.46
6900r/1901r[a]	83.18	46.34	91.99	227.27	79.24
6913r/6914r[a]	76.67	59.42	92.42	230.55	97.61
7052r	83.01	56.85	92.20	235.09	85.00

[a] These images were mosaicked together to create a complete image of the area.

Appendix B. Photometric correction applied to *Galileo* images

The two-term Henyey-Greenstein (2T-HG) photometric function was applied to each image, defined by the following function:

$$P(\alpha) = \frac{(1+c)}{2}\frac{1-b^2}{(1+2b\cos\alpha+b^2)^{\frac{3}{2}}} + \frac{(1-c)}{2}\frac{1-b^2}{(1-2b\cos\alpha+b^2)^{\frac{3}{2}}}$$

In this equation, α represents the phase angle of an image, b is the approximate widths of the two independent scattering lobes, and f is the partition coefficient. The values for the parameters named here are c = 0.113 for the leading hemisphere, c = 0.391 for the trailing hemisphere, b = −0.429 for the leading hemisphere, and b = −0.443 for the trailing hemisphere (Domingue et al., 1990). The differences between the parameters for the leading and trailing hemispheres are due to the increased amount of ionic bombardment present on the trailing hemisphere. Multiple studies (Hartman and Domingue, 1998; Shepard and Helfenstein, 2007) show that there is no improvement in the model fit between the 2T-HG function over the three-term Henyey-Greenstein (3T-HG) function when phase angles are < 130°; hence, we opted for the simpler 2T-HG equation.

References

Anderson, J.A., et al., 2004. Modernization of the integrated software for imagers and spectrometers. Lunar Planet. Sci. XXXV (Houston, Texas, Abstract #2039).

Bayer, T., et al., 2018. Europa Clipper mission update: Preliminary design with selected instruments. In: IEEE Aerospace Conference. 8396629.

Belton, M.J.S., et al., 1992. The Galileo solid-state imaging experiment. Space Sci. Rev. 60, 413–455.

Bunte, M.K., 2013. Utilizing Science and Technology to Enhance a Future Planetary Mission: Applications to Europa (Ph.D. thesis). Arizona State University, Tempe, Arizona (279 pp).

Carlson, R.W., Anderson, M.S., Mehlman, R., Johnson, R.E., 2005. Distribution of hydrate on Europa: further evidence for sulfuric acid hydrate. Icarus 177, 461–471.

Carlson, R.W., et al., 2009. Europa's surface composition. In: Pappalardo, R.T., McKinnon, W.B., Khurana, K.K. (Eds.), Europa. The University of Arizona Press, Tucson, pp. 283–327.

Carr, M. H., et al., 1998. Evidence for a subsurface ocean on Europa. Nature 391, 363–365.

Collins, G., Nimmo, F., 2009. Chaotic terrain on Europa. In: Pappalardo, R.T., McKinnon, W.B., Khurana, K.K. (Eds.), Europa. The University of Arizona Press, Tucson, pp. 259–281.

Collins, G.C., Head, J.W., Pappalardo, R.T., Spaun, N.A., 2000. Evaluation of models for the formation of chaotic terrain on Europa. J. Geophys. Res. 105, 1709–1716.

Craft, K.L., Patterson, G.W., Lowell, R.P., Germanovich, L., 2016. Fracturing and flow: investigations on the formation of shallow water sills on Europa. Icarus 274, 297–313.

Culha, C., Manga, M., 2016. Geometry and spatial distribution of lenticulae on Europa. Icarus 271, 49–56.

Dalton, J.B., Prieto-Ballesteros, O., Kargel, J.S., Jamieson, C.S., Jolivet, J., Quinn, R., 2005. Spectral comparison of heavily hydrated salts with disrupted terrains on Europa. Icarus 177, 472–490.

Doggett, T., Greeley, R., Figueredo, P., Tanaka, K., 2009. Geologic stratigraphy and evolution of Europa's surface. In: Pappalardo, R.T., McKinnon, W.B., Khurana, K.K. (Eds.), Europa. The University of Arizona Press, Tucson, pp. 137–159.

Domingue, D.L., Hapke, B.W., Lockwood, G.W., Thompson, D.T., 1990. Europa's phase curve: implications for surface structure. Icarus 90, 30–42.

Fagents, S.A., 2003. Considerations for effusive cryovolcanism on Europa: the post-Galileo perspective. J. Geophys. Res. 108. https://doi.org/10.1029/2003JE002128.

Figueredo, P.H., Greeley, R., 2004. Resurfacing history of Europa from pole-to-poke geological mapping. Icarus 167, 287–312.

Figueredo, P.H., Chuang, F.C., Rathbun, J., Kirk, R.L., Greeley, R., 2002. Geology and origin of Europa's "mitten" feature (Murias Chaos). J. Geophys. Res. 107. https://doi.org/10.1027/2001JE001591.

Greeley, R., et al., 1998. Europa: initial Galileo geological observations. Icarus 135, 4–24.

Greeley, R., et al., 2000. Geologic mapping of Europa. J. Geophys. Res. 105, 22559–22578.

Greenberg, R., Hoppa, G.V., Tufts, B.R., Geissler, P., Riley, J., Kadel, S., 1999. Chaos on Europa. Icarus 141, 263–286.

Greenberg, R., Leake, M.A., Hoppa, G.V., Tufts, B.R., 2003. Pits and uplifts on Europa. Icarus 161, 102–126.

Han, L., Showman, A.P., 2005. Thermo-compositional convection in Europa's icy shell with salinity. Geophys. Res. Lett. 32. https://doi.org/10.1029/2005GL023979.

Han, L., Showman, A.P., 2010. Coupled convection and tidal dissipation in Europa's ice shell. Icarus 207, 834–844.

Hand, K.P., Carlson, R.W., 2015. Europa's surface color suggests an ocean rich with sodium chloride. Geophys. Res. Lett. 42, 3174–3178.

Hartman, B., Domingue, D., 1998. Scattering of light by individual particles and the implications for models of planetary sciences. Icarus 131, 421–448.

Head, J.W., Pappalardo, R.T., 1999. Brine mobilization during lithospheric heating on Europa: implications for formation of chaos terrain, lenticula texture, and color variations. J. Geophys. Res. 104, 27143–27155.

Head, J. W., et al., 1999. Europa: recent geological history from Galileo observations. Lunar Planet. Sci. XXX, 1404 (abstract).

Jenness, J., 2011. Tools for Graphics and Shapes [Computer Software]. Version 2.1.85. Retrieved from. http://www.jennessent.com/arcgis/shapes_graphics.htm.

Leonard, E.J., Patthoff, D.A., Senske, D., Collins, G.C., 2017. The first USGS geologic map of Europa. In: American Geophysical Union Fall Meeting 2017, (Abstract #P33A-2862).

Leonard, E.J., Collins, G., Senske, D., Patthoff, D.A., 2018. The global geology of Europa: units, their distribution, and implications for formation processes. In: COSPAR Sci. Assem. XLII (B5.3-14-18, abstract).

Manga, M., Wang, C.-Y., 2007. Pressurized oceans and the eruption of liquid water on Europa and Enceladus. Geophys. Res. Let. 34. https://doi.org/10.1029/2007GL029297.

Manga, M., Michaut, C., 2017. Formation of lenticulae on Europa by saucer-shaped sills. Icarus 286, 261–269.

McCord, T.B., Teeter, G., Hansen, G.B., Sieger, M.T., Orlando, T.M., 2002. Brines exposed to Europa surface conditions. J. Geophys. Res. 107. https://doi.org/10.1029/2000JE001453.

Michaut, C., Manga, M., 2014. Domes, pits, and small chaos on Europa produced by water sills. J. Geophys. Res. 119, 550–573. https://doi.org/10.1002/2013JE004558.

Mitri, G., Showman, A.P., 2008. A model for the temperature-dependence of tidal dissipation in convection plumes on icy satellites: implications for Europa and Enceladus. Icarus 195, 758–764.

Neish, C.D., Prockter, L.M., Patterson, G.W., 2012. Observational constraints on the identification and distribution of chaotic terrain on icy satellites. Icarus 221, 72–79.

Nimmo, F., Giese, B., 2005. Thermal and topographic tests of Europa chaos formation models from Galileo E15 observations. Icarus 177, 327–340.

Noviello, J.L., Rhoden, A.R., 2018. Identification of microfeatures on Europa in low-

resolution Galileo images: successes, limits, and implications for Europa's exploration. Lunar Planet. Sci. XLIX, 2707 (abstract).
Noviello, J.L., Rhoden, A.R., Torrano, Z.A., Manga, M., 2017. The inferred distribution of liquid water in Europa's ice shell: implications for the Europa Lander Mission. Am. Geophys. Union XCIX, 232681 (abstract).
O'Brien, D.P., Geissler, P., Greenberg, R., 2002. A melt-through model for chaos formation on Europa. Icarus 156, 152–161.
Ojakangas, G.W., Stevenson, D.J., 1989. Thermal state of an ice shell on Europa. Icarus 81, 220–241.
Pappalardo, R.T., Barr, A.C., 2004. The origin of domes on Europa: the role of thermally induced compositional diapirism. Geophys. Res. Lett. 31. https://doi.org/10.1029/2003GL019202.
Pappalardo, R. T., et al., 1998. Geological evidence for solid-state convection in Europa's ice shell. Nature 391, 365–368.
Pappalardo, R. T., et al., 1999. Does Europa have a subsurface ocean? Evaluation of the geological evidence. J. Geophys. Res. 104. 24015–25055.
Pappalardo, R.T., et al., 2016. Lunar Planet. Sci. XLVII. pp. 3058 (abstract).
Phillips, C.B., Pappalardo, R.T., 2014. Europa Clipper mission concept: exploring Jupiter's ocean moon. Eos 95, 165–167 (No. 20).
Prockter, L.M., Schenk, P., 2005. Origin and evolution of Castalia Macula, an anomalous young depression on Europa. Icarus 177, 305–326.
Prockter, L.M., et al., 1999. Europa: stratigraphy and geological history of the anti-Jovian region from Galileo E14 solid-state imaging data. J. Geophys. Res. 104 (16), 16,531–16,540.
Quick, L.C., Marsh, B.D., 2016. Heat transfer of ascending cryomagma on Europa. J. Volcanol. Geotherm. Res. 319, 66–77.
Quick, L.C., Glaze, L.S., Baloga, S.M., 2017. Cryovolcanic emplacement of domes on Europa. Icarus 284, 477–488.
Rathbun, J.A., Musser, G.S., Squyres, S.W., 1998. Ice diapirs on Europa: implications for liquid water. Geophys. Res. Lett. 25, 4157–4160.
Riley, J., Hoppa, G.V., Greenberg, R., Tufts, B.R., Geissler, P., 2000. Distribution of chaotic terrain on Europa. J. Geophys. Res. 105, 22599–22615.
Schenck, P., Matsuyama, I., Nimmo, F., 2008. True polar wander on Europa from global-scale small-circle depressions. Nature 453, 368–371.
Schenk, P.M., Pappalardo, R.T., 2004. Topographic variations in chaos on Europa: implications for diapiric formation. Geophys. Res. Lett. 31. https://doi.org/10.1029/2004GL019978.
Schmidt, B.E., Blankenship, D.D., Patterson, G.W., Schenk, P.M., 2011. Active formation of 'chaos terrain' over shallow subsurface water on Europa. Nature 479, 502–505.
Shepard, M.K., Helfenstein, P., 2007. A test of the Hapke photometric model. J. Geophys. Res. 112. https://doi.org/10.1029/2005JE002625.
Showman, A.P., Han, L., 2004. Numerical simulations of convection in Europa's ice shell: implications for surface features. J. Geophys. Res. 109. https://doi.org/10.1029/2003JE002103.
Showman, A.P., Han, L., 2005. Effects of plasticity of convection in Europa's ice shell: implications for surface features. Icarus 177, 425–437.
Singer, K.N., McKinnon, W.B., Schenk, P.M., 2010. Pits, spots, uplifts, and small chaos regions on Europa: evidence for diapiric upwelling from morphology and morphometry. Lunar Planet. Sci. XLI, 2195 (abstract).
Singer, K.N., McKinnon, W.B., Schenk, P.M., 2019. Pits, uplifts and small chaos features on Europa: evidence for diapiric upwelling from morphology and morphometry. Icarus (in review, submitted for publication).
Snyder, J.P., Voxland, P.M., 1994. An album of map projections. U. S. Geol. Surv. Prof. Pap. 1453.
Soderlund, K.M., Schmidt, B.E., Wicht, J., Blankenship, D.D., 2014. Ocean-driven heating of Europa's icy shell at low latitudes. Nat. Geosci. 7, 16–19. https://doi.org/10.1038/NGEO02021.
Sotin, C., Head, J.W., Tobie, G., 2002. Europa: tidal heating of upwelling thermal plumes and the origin of lenticulae and chaos melting. Geophys. Res. Lett. 29 (DOI:0094-8276/02/2001GL013844).
Spaun, N.A., 2002. Chaos, Lenticulae, and Lineae on Europa: Implications for Geological History, Crustal Thickness, and the Presence of an Ocean (Ph.D. thesis). Brown University, Providence, Rhode Island.
Spaun, N.A., Head, J.W., Collins, G.C., Prockter, L.M., Pappalardo, R.T., 1998. Conamara Chaos region, Europa: reconstruction of mobile polygonal ice blocks. Geophys. Res. Lett. 25, 4277–4280.
Spaun, N.A., Prockter, L.M., Pappalardo, R.T., Head, J.W., Collins, G.C., Antman, A., Greeley, R., 1999. Spatial distribution of lenticulae and chaos on Europa. Lunar Planet. Sci. XXX, 1847 (abstract).
Spaun, N.A., Head, J.W., Pappalardo, R.T., 2004. Europan chaos and lenticulae: a synthesis of size, spacing, and areal density analyses. Lunar Planet. Sci. XXXV, 1409 (abstract).
Tognetti, L., Rhoden, A., Nelson, D., 2017. Investigating a link between large and small-scale chaos features on Europa. In: American Geophysical Union Fall Meeting 2017, Abstract #P43C-2904.
Torson, J.M., Becker, K.J., 1997. ISIS - a software architecture for processing planetary images. Lunar Planet. Sci. XXVIII (Houston, Texas, Abstract #1219).
Turtle, E.P., et al., 2016. The Europa imaging system (EIS): high-resolution imaging and topography to investigate Europa's geology, ice shell, and potential for current activity. Lunar Planet. Sci. XLVII (Houston, Texas, Abstract #1626).
U.S. Geological Survey, 2002. Controlled Photomosaic Map of Europa, Je15M CMN: U.S. Geological Survey Geologic Investigations Series I–2757. available at. http://pubs.usgs.gov/imap/i2757/.